Effect of Coordinate Switching on Simulation Accuracy of Translunar Trajectories

Except where reference is made to the work of others, the work described in this thesis is my own or was done in collaboration with my advisory committee. This thesis does not include proprietary or classified information.

Mana P. Vautier

Certificate of Approval:

John E. Cochran, Jr.
Department Head and Professor
Aerospace Engineering

Andrew J. Sinclair, Chair
Assistant Professor
Aerospace Engineering

David A. Cicci
Professor
Aerospace Engineering

Joe F. Pittman
Interim Dean
Graduate School

Effect of Coordinate Switching on Simulation Accuracy of Translunar Trajectories

Mana P. Vautier

A Thesis

Submitted to

the Graduate Faculty of

Auburn University

in Partial Fulfillment of the

Requirements for the

Degree of

Master of Science

Auburn, Alabama
09 August, 2008

Effect of Coordinate Switching on Simulation Accuracy of Translunar Trajectories

Mana P. Vautier

Permission is granted to Auburn University to make copies of this thesis at its discretion, upon the request of individuals or institutions and at their expense. The author reserves all publication rights.

_____

Signature of Author

_____

Date of Graduation

Vita

Mana Vautier, son of Ian Philip and Hinekaitangi Awhi (Skipwith) Vautier, was born 5 February, 1980, in Auckland, New Zealand. He graduated from Saint Kentigern College in 1997 and attended the University of Auckland for one year. In 2003 he transferred to Brigham Young University in Provo, Utah and graduated with a Bachelor of Science degree in Physics-Astronomy. He began his graduate studies in Aerospace Engineering at Auburn University in August 2006. In August 2004 he married Annette (Hughes) Vautier, daughter of Eugene Marion and Constance (Huffman) Hughes. They have two sons, Michael and Benjamin.

Figure 1: My Family.

Thesis Abstract

Effect of Coordinate Switching on Simulation Accuracy of Translunar Trajectories

Mana P. Vautier

Master of Science, 09 August, 2008
(B.S., Brigham Young University, 2006)

70 Typed Pages

Directed by Andrew J. Sinclair

This thesis focuses on the effect of round-off error in the accurate simulation of translunar trajectories. The three-body dynamics can be posed in either an Earth-centered (EC) or Moon-centered (MC) frame. In this study, multiple translunar trajectories were simulated to determine if there is an optimal switch point from an EC to MC frame that minimizes round-off error. A high fidelity baseline simulation was first created, and the entire trajectory was propagated in EC. Comparison trajectories were then simulated at lower precision using both EC and MC frames. The trajectory was propagated first in EC and then switched to MC at a preselected switch point. By testing a range of switch points, it was determined that switching to the MC frame during the first 10% of the trajectory led to significantly higher round-off errors. For any later switch points, there was little sensitivity in the round-off error. There was, however, some correlation to switch points located at the radii of well established gravitational spheres of the Moon. The importance of round-off error in simulation of translunar trajectories is also demonstrated by calculation of the Lyapunov exponents along the trajectory.

Acknowledgments

I would like to acknowledge all my professors who helped me get to where I am today. I am especially grateful to my advisor, Dr. Andrew Sinclair, for his constant encouragement, guidance and support. He went above and beyond to help me succeed in my graduate studies, while still having fun with the BBQ's, the Biscuits and the Wartburg Warts (who came up with that name anyway?). I also want to acknowledge Odyssey Space Research, L.L.C. who took me on as an intern during the summer of 2007, during which time the idea for my research was first inspired. I must also mention my fellow graduate students with whom I shared the last two years. Their friendship, humour and timely help made even the toughest assignments bearable. Much deserved gratitude also goes to my parents and family for their unending love and support throughout my entire career as a full-time student (all 20 years worth!). My parents instilled in me the belief that I could do anything if I worked hard and truly put my mind to it, and my siblings never failed to help me feel brainy while making sure my head never got too big. I want to express my love and gratitude to Michael and Benjamin, two of the best sons a father could hope for. Their infectious laughter, their love of life, and their joy in the simple things served as a constant reminder as to what is most important in life. Finally, I want to acknowledge my sweet angel wife, Annette. She is truly a light in my life, and I am forever grateful for her continual patience, encouragement and love. She has stood by my side through the thick and the thin, the good and the bad, the easy and the rough. I take much joy in knowing that together we stand side-by-side as eternal companions through this great journey called life.

Style manual or journal used Journal of Approximation Theory (together with the style known as "aums"). Bibliograpy follows van Leunen's *A Handbook for Scholars.*

Computer software used The document preparation package TEX (specifically LATEX) together with the departmental style-file `aums.sty`.

Table of Contents

List of Figures x

List of Tables xi

1 Introduction 1

2 System Model 3

3 Gravitational Spheres 10
3.1 Sphere of Gravitation 11
3.2 Sphere of Influence 12
3.3 Hill Sphere 15
3.4 Kislik Sphere 17

4 Chaos 20
4.1 Historical Perspective 20
4.2 Chaos Theory and Dynamic Systems 22
4.3 Lyapunov Exponents 24
4.4 State Transition Matrix 29

5 Simulation Model 31

6 Results 38

7 Discussion 46
7.1 Conclusion 46
7.2 Future Work 47

Bibliography 48

Appendices 50

A MATLAB Code 51
A.1 Double Precision Simulation 51
A.2 Single Precision Simulation 52
A.3 Sub-Routines 54

B Historical Review 56
B.1 Claudius Ptolemaeus 56
B.2 Nicolaus Copernicus 56
B.3 Galileo Galilei 56
B.4 Johannes Kepler 56
B.5 Isaac Newton 57
B.6 Joseph Louis Lagrange 57
B.7 Pierre-Simon Laplace 57
B.8 Henri Poincaré 58
B.9 Aleksandr Lyapunov 58

Index 59

List of Figures

1 My Family iv

2.1 Position vectors 8

3.1 Sphere of Influence size variance 14

3.2 Zero velocity curves 16

4.1 Evolution of Lorenz's experiment 21

4.2 Bifurcation diagram for the Logistic map 23

4.3 The Lorenz Attractor 24

4.4 Evolution of a hypersphere 27

5.1 System model position vectors 31

5.2 Translunar trajectory 33

5.3 Schematic of initial conditions 34

6.1 Acceleration ratios 38

6.2 RSS position error 39

6.3 RSS error for three switch points 40

6.4 RMS values 41

6.5 Magnified RMS values 42

6.6 Representation of simulation results 43

6.7 Lyapunov Exponents 44

6.8 Spacecraft range 45

List of Tables

3.1 Radii of Gravitational Spheres 19

5.1 Physical Parameters of the Simulation Model 35

6.1 Gravitational Spheres and Switch Point Times 43

Chapter 1

Introduction

NASA's Project Constellation is committed to the long-term human and robotic exploration of the Moon, Mars, and beyond. Although the spacecraft developed will still have the capability of delivering payload to Low Earth Orbit (LEO) , there is a renewed emphasis on leaving the gravitational influence of the Earth, and traveling to the Moon. Compared to the era of the Apollo missions, numerical simulations have grown in capability and importance. As a result, simulation accuracy has also improved significantly, and numerical results can now be calculated with much greater precision. Until recently, these more advanced tools have primarily been used in simulating LEO's. The new focus on lunar missions, however, motivates the development of precise translunar simulations.

The issue of model choices affects the numerical error in the simulation of translunar trajectories. Numerical errors typically include several sources such as discretization error, round-off error, and iterative error. This work presents an investigation of the role of coordinate choice in reducing round-off error to improve simulation accuracy. The importance of round-off error in the simulation accuracy will also be investigated by demonstrating the chaotic nature of the trajectories.

Chapter 2 discusses the three-body problem and representations of the spacecraft trajectory. Chapter 3 presents an overview of four definitions for a gravitational sphere. Chapter 4 introduces the concept of chaos theory and the sensitivity of a trajectory to initial conditions. The specific model used for the simulations in this study are presented in Chapter 5, and results are given in Chapter 6. Finally, a

discussion of possible future work is found in Chapter 7 along with some concluding remarks.

Chapter 2

System Model

Published in 1687, Sir Isaac Newton's *Philosophiæ Naturalis Principia Mathematica* or more simply, the *Principia*, is considered by many historians to be one of the supreme achievements of the human mind [1]. In it, he introduced the three laws of motion which help describe most non-relativistic dynamical systems.

By letting $\mathbf{r}$, $\mathbf{v}$ and $\mathbf{a}$ respectively denote the position, velocity and acceleration of a body of mass m from a fixed origin so that

$$\mathbf{v} = \frac{d\mathbf{r}}{dt} \quad \text{and} \quad \mathbf{a} = \frac{d\mathbf{v}}{dt} = \frac{d^2\mathbf{r}}{dt^2}, \tag{2.1}$$

Newton's first and second laws can be summarized by the mathematical expression

$$\mathbf{F} = \frac{d(m\mathbf{v})}{dt} \tag{2.2}$$

where $\mathbf{F}$ is the impressed force acting on the body. Assuming that the body's mass is constant, equation (2.2) can then be generalized for the case where n multiple external forces are acting on the system producing

$$\sum_{i=1}^{n} \mathbf{F}_i = m_i \frac{d^2\mathbf{r}_i}{dt^2}. \tag{2.3}$$

Also the third law, again in vector notation, can be expressed mathematically by

$$\mathbf{F}_1 = -\mathbf{F}_2. \tag{2.4}$$

These three laws of motion enunciated by Newton laid the foundations of the field of dynamics.

Another significant scientific contribution made by Newton was his formulation of the law of universal gravitation. This law can be stated quite simply that every particle in the universe is simultaneously attracted to every other particle in the universe with a gravitational force which is directly proportional to the product of the masses and inversely proportional to the square of the distance between them. Thus, for any two bodies, we can express the magnitude of this force by the relationship

$$F = G\frac{m_1 m_2}{r^2} \tag{2.5}$$

where F is the magnitude of the gravitational force of attraction between masses m_1 and m_2 which are separated by a distance r. The proportionality factor, G, is known as the constant of universal gravitation and has a value of $(6.6741 \pm 0.0008) \times 10^{-11}$ $\mathrm{m}^3/(\mathrm{kg} \cdot \mathrm{s}^2)$ [2]. Although this law holds true specifically for point mass particles, it also holds for spherical bodies whose masses are evenly distributed. Since most planets and stars can be approximated as such, Newton's law of universal gravitation has formed the basis of celestial mechanics, as well as the more modern field of astrodynamics.

One of the most fundamental problems of astrodynamics is to accurately describe the motion of n gravitationally interacting massive particles. Obviously the most simplistic scenario occurs when $n = 2$, and is known as the two-body problem. This problem states, 'Given the position and velocity of two massive particles at any time, calculate their position and velocity for any other time.' The significance of this problem lies in the two main facts that a) it is the only problem in gravitational

dynamics for which a general analytical solution is obtainable, and b) it can be used as an approximation for a wide variety of multi-body orbital problems.

A more general n-body problem can be stated by considering a system of n point masses $m_1, m_2, m_3, ..., m_n$. An analytical description of the interactions and resulting motion of these bodies can be provided using the four previously mentioned laws published by Newton. Assume a suitable inertial coordinate system in which the positions of the n masses are given by

$$\mathbf{r}_i = x_i\mathbf{i}_x + y_i\mathbf{i}_y + z_i\mathbf{i}_z \qquad (i = 1, 2, 3, ..., n)$$

where $\mathbf{i}_x$, $\mathbf{i}_y$, and $\mathbf{i}_z$ represent the respective unit vectors along the x, y and z coordinate axes. Applying Newton's law of universal gravitation, the magnitude of the force of attraction exerted on m_i by m_j is

$$F_i = G\frac{m_i m_j}{r_{ij}^2} \qquad (i = 1, 2, 3...n \quad j = 1, 2, 3, ..., n \quad j \neq i) \tag{2.6}$$

where

$$r_{ij} = |\mathbf{r}_j - \mathbf{r}_i| = \sqrt{(\mathbf{r}_j - \mathbf{r}_i) \cdot (\mathbf{r}_j - \mathbf{r}_i)}.$$

The direction of the force can be conveniently expressed by multiplying equation (2.6) by the unit vector directed along the line of centers of the two masses m_i and m_j to obtain

$$\mathbf{F}_i = G\frac{m_i m_j}{r_{ij}^2}\frac{\mathbf{r}_{ij}}{|\mathbf{r}_{ij}|} \tag{2.7}$$

where

$$\mathbf{r}_{ij} = \mathbf{r}_j - \mathbf{r}_i = -\mathbf{r}_{ji}.$$

Then, by summing all such gravitational forces acting on the i^{th} body

$$\mathbf{F}_i = G\frac{m_i m_1}{r_{i1}^3}\mathbf{r}_{i1} + G\frac{m_i m_2}{r_{i2}^3}\mathbf{r}_{i2} + ... + G\frac{m_i m_n}{r_{in}^3}\mathbf{r}_{in}. \tag{2.8}$$

Since the i^{th} body cannot exert a force upon itself, equation (2.8) does not include the term $G\frac{m_i m_i}{r_{ii}^3}\mathbf{r}_{ii}$ and can be simplified using the summation notation such that

$$\mathbf{F}_i = G\sum_{j=1}^{n}\frac{m_i m_j}{r_{ij}^3}\mathbf{r}_{ij} \qquad (i\text{=}1,2,3,...,n \quad \text{and} \quad j \neq i). \tag{2.9}$$

Now applying Newton's second law of motion

$$m_i\frac{d^2\mathbf{r}_i}{dt^2} = G\sum_{j=1}^{n}\frac{m_i m_j}{r_{ij}^3}\mathbf{r}_{ij} \qquad (i\text{=}1,2,3,...,n \quad \text{and} \quad j \neq i). \tag{2.10}$$

Finally, canceling m_i from both sides gives the second order, non-linear, vector differential equation of motion for the i^{th} body of the system of n particles all acting under their mutual gravitational attractions.

$$\frac{d^2\mathbf{r}_i}{dt^2} = G\sum_{j=1}^{n}\frac{m_j}{r_{ij}^3}\mathbf{r}_{ij} \qquad (i\text{=}1,2,3,...,n \quad \text{and} \quad j \neq i). \tag{2.11}$$

By setting $n = 2$, it is a relatively simple matter to reduce equation (2.11) to an expression for only two bodies. When coupled with a set of initial conditions for the positions and velocities at time t_0, the motion of the two bodies is fully described, and the positions and velocities at any future time t may be calculated. This forms the solution to the famous two-body problem stated and solved by Newton.

For the case where $n > 2$ however, a solution is not so easily obtained. By the end of the nineteenth century, it was considered an important and challenging enough question that for his 60^{th} birthday, Oscar II, King of Sweden, announced that a prize would be given to anyone who could find the solution to the problem. The

specific announcement was: "Given a system of arbitrarily many mass points that attract each according to Newton's law, under the assumption that no two points ever collide, try to find a representation of the coordinates of each point as a series in a variable that is some known function of time and for all of whose values the series converges uniformly" [3].

In case the problem could not be solved, any other important contribution to celestial mechanics would then be considered to be prizeworthy. The prize was finally awarded to Henri Poincaré, even though he did not solve the original problem. One of the judges, the distinguished Karl Weierstrass, said, "This work cannot indeed be considered as furnishing the complete solution of the question proposed, but that it is nevertheless of such importance that its publication will inaugurate a new era in the history of celestial mechanics." The seminal work produced by Poincaré would later lead to the development of chaos theory as discussed in Chapter 4.

It will be instructive here to develop the differential equations of relative motion for the three-body problem. We have from equation (2.11) the relation

$$\frac{d^2\mathbf{r}_i}{dt^2} = G\sum_{j=1}^{n}\frac{m_j}{r_{ij}^3}\mathbf{r}_{ij} \qquad (i=1,2,3...n \quad \text{and} \quad j \neq i) \tag{2.12}$$

Now let the reference body be mass m_1. Its equation of motion with respect to an inertial (unaccelerated) coordinate frame is then

$$\frac{d^2\mathbf{r}_1}{dt^2} = G\frac{m_2}{r_{12}^3}\mathbf{r}_{12} + G\frac{m_3}{r_{13}^3}\mathbf{r}_{13}, \tag{2.13}$$

while the equation of motion for m_2 in the same coordinate axes is

$$\frac{d^2\mathbf{r}_2}{dt^2} = G\frac{m_1}{r_{21}^3}\mathbf{r}_{21} + G\frac{m_3}{r_{23}^3}\mathbf{r}_{23}. \tag{2.14}$$

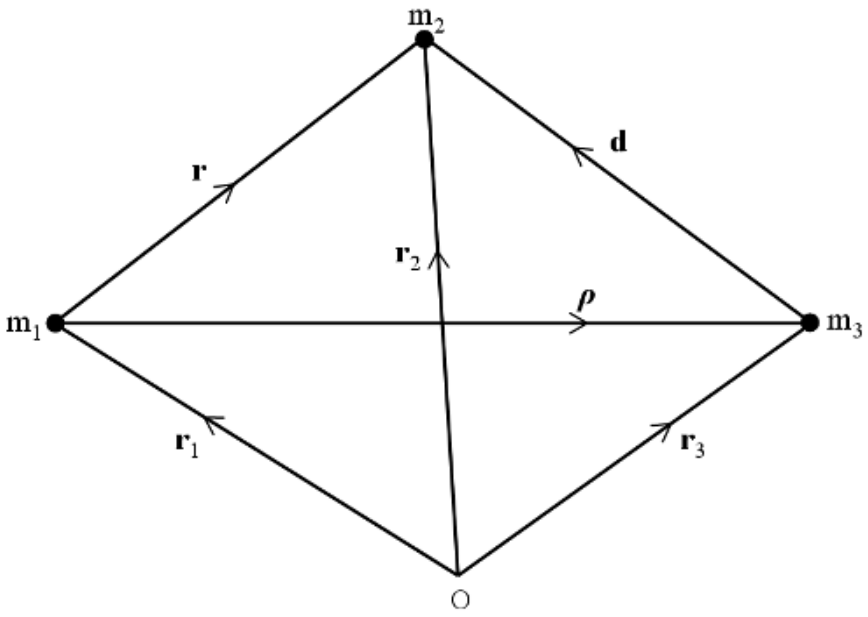

Figure 2.1: System model position vectors.

By subtracting equation (2.13) from (2.14), the motion of m_2 relative to m_1 is obtained

$$\frac{d^2\mathbf{r}_2}{dt^2} - \frac{d^2\mathbf{r}_1}{dt^2} = G\left[\frac{m_1}{r_{21}^3}\mathbf{r}_{21} - \frac{m_2}{r_{12}^3}\mathbf{r}_{12} + \frac{m_3}{r_{23}^3}\mathbf{r}_{23} - \frac{m_3}{r_{13}^3}\mathbf{r}_{13}\right]. \tag{2.15}$$

Now define the following variables

$$\mathbf{r} \equiv \mathbf{r}_2 - \mathbf{r}_1 \quad \boldsymbol{\rho} \equiv \mathbf{r}_3 - \mathbf{r}_1 \quad \mathbf{d} \equiv \mathbf{r}_2 - \mathbf{r}_3 \tag{2.16}$$

as shown in Fig. 2.1 where $\mathbf{r_1}$, $\mathbf{r_2}$ and $\mathbf{r_3}$ are position vectors from an inertial reference point, O, to the corresponding masses m_1, m_2 and m_3. By factoring appropriate terms and noting that $\mathbf{r}_{ij} = \mathbf{r}_j - \mathbf{r}_i$, equation (2.15) can be simplified to

$$\frac{d^2\mathbf{r}}{dt^2} + \frac{G(m_1 + m_2)}{r^3}\mathbf{r} = -Gm_3\left(\frac{1}{d^3}\mathbf{d} + \frac{1}{\rho^3}\boldsymbol{\rho}\right). \tag{2.17}$$

Following a similar process, the motion of m_2 relative to m_3 can shown to be

$$\frac{d^2\mathbf{d}}{dt^2} + \frac{G(m_2 + m_3)}{d^3}\mathbf{d} = -Gm_1\left(\frac{1}{r^3}\mathbf{r} - \frac{1}{\rho^3}\boldsymbol{\rho}\right). \tag{2.18}$$

In both instances, the second term on the left hand side corresponds to the central acceleration due to the primary body, while the term on the right hand side is associated with the disturbing force from the perturbing body.

It is also worthwhile to mention that there exists many other external forces that may act upon any given body, other than the gravitational forces described above. These forces, known as perturbations, may include, but are not limited to, atmospheric drag, thrusting, solar radiation pressure, outgassing and charged or uncharged particles. One of the most significant perturbations is due to non-sphericity of the bodies. As noted previously, Newton's law of gravitation applies only if the mass of a body is evenly distributed in homogenous spherical shells. For this reason, the expressions derived above are approximations, and the inclusion of additional perturbing forces could more accurately model the true trajectory.

Chapter 3

Gravitational Spheres

There are many applications in which the n-body problem may be broken down into a series of two-body problems, particularly for the case when the mass of the primary body is much greater than the mass of all other bodies considered in the system. Implementing this method provides an appropriate first approximation to the determination of precise spacecraft orbits.

In many such cases, the true trajectory of the spacecraft is represented by an approximate one composed of a sequence of conic sections, constructed by deriving solutions of individual two-body problems in a particular sequence throughout the trajectory. For example, if a spacecraft were traveling from the Earth to Mars, the journey can be modeled by first treating the trajectory as a two-body system composed of the Earth and the spacecraft. At some point, the trajectory is modeled by switching to the spacecraft-sun two-body system, and finally as the spacecraft approaches Mars, the solution to the spacecraft-Mars two-body system is used.

This particular method is known as the *patched-conic approximation*, and despite the fact that it is only an approximation to true trajectory, it does afford a convenient means of investigating various initial and boundary conditions, while avoiding lengthy computation times. The obvious question then, is at what point along the trajectory should the reference frame be switched such that the terminal position and velocity of one section is equivalent to the initial position and velocity of the next section.

The concept of a gravitational sphere introduces the notion that there is a certain region of space associated with any given body. In celestial mechanics, there have been

many different approaches to constructing these gravitational spheres, the boundaries of which can be examined as a possible location for an optimal switch point.

3.1 Sphere of Gravitation

The definition of a gravitational sphere most directly related to the gravitational forces between two bodies is that derived by Gurzadyan [4]. Consider two celestial bodies of masses m_1 and m_3. It is evident that a spacecraft of mass m_2 will be influenced by gravitational forces from both such bodies. If it is assumed that the spacecraft is stationary and located on the vector line $\boldsymbol{\rho}$, then there always exists a distance d from m_3 at which the gravitational accelerations exerted by both bodies on the spacecraft will be equal to each other. Mathematically this relationship can be expressed by

$$F_{23} = F_{12}.$$

Then from equation (2.5)

$$G\frac{m_2 m_3}{d^2} = G\frac{m_1 m_2}{r^2}. \tag{3.1}$$

Now setting $d = R_{g_1}$, and substituting in $r = \rho - R_{g_1}$

$$\begin{aligned} m_3(\rho - R_{g_1})^2 &= m_1 R_{g_1}^2 \\ \frac{\rho - R_{g_1}}{R_{g_1}} &= (m_1/m_3)^{1/2} \\ \rho - R_{g_1} &= R_{g_1}(m_1/m_3)^{1/2} \\ \rho &= R_{g_1}\left(1 + (m_1/m_3)^{1/2}\right) \end{aligned} \tag{3.2}$$

which can easily be solved for R_{g_1}, producing the simple expression for the radius of the sphere of gravitation

$$R_{g_1} = \frac{\rho}{1 + (m_1/m_3)^{1/2}}. \tag{3.3}$$

Rauschenbakh *et al.* [5] refer to the sphere of gravitation as the *sphere of attraction* and make the further simplifying assumption that $m_1 >> m_3$. By virtue of this assumption, the radius of the gravitational sphere lies at a small enough distance from m_3 such that $r \approx \rho$. Under this simplifying condition, and setting $d = R_{g_2}$, equation (3.1) is reduced to

$$R_{g_2} = \rho\sqrt{\frac{m_3}{m_1}}. \tag{3.4}$$

Chebotarev [6], who defines his sphere of gravitation identically to Rauschenbakh *et al.*, makes the interesting observation that of all the satellites of the major planets, only the Earth's moon is at all times beyond the limits of the sphere of gravitation of the planet. This suggests that the Moon should be attracted more strongly by the Sun than by the Earth. Indeed, if the Moon were to suddenly stop its motion, it would fall onto the Sun, and not the Earth around which it orbits. Of course such a scenario is not feasible, and herein lies the limitation to the significance of the concept of the sphere of gravitation, since neither do bodies at absolute rest exist nor can they be suddenly stopped.

3.2 Sphere of Influence

Pierre-Simon Laplace, an 18th century mathematician and astronomer, considered the accurate computation of the motion of a comet which approaches very near

to a disturbing planet. He hypothesized that "if the planet be Jupiter, its attraction upon the comet may exceed that of the sun, and this action can entirely change the elements of its orbit. This singular case, which appears to have taken place with the first comet of the year 1770, deserves particular attention" [7].

By introducing the four acceleration vectors $\mathbf{C}_1$, $\mathbf{P}_1$, $\mathbf{C}_3$ and $\mathbf{P}_3$ to respectively represent the central and perturbing accelerations of mass m_2 with respect either m_1 or m_3, equations (2.17) and (2.18) can be rewritten as

$$\frac{d^2\mathbf{r}}{dt^2} + \mathbf{C}_1 = \mathbf{P}_3 \tag{3.5}$$

and

$$\frac{d^2\mathbf{d}}{dt^2} + \mathbf{C}_3 = \mathbf{P}_1. \tag{3.6}$$

According to Laplace, the advantage of equation (3.5) over (3.6), or vice-versa, is dependant upon the ratio of the disturbing acceleration to the central acceleration. The idea is to select the appropriate central body so that the patched-conic approximation can be applied in a reference frame in which the perturbing acceleration is less, thereby maximizing the accuracy of the computation. The boundary defined by the equality of these two ratios

$$\frac{|\mathbf{P}_3|}{|\mathbf{C}_1|} = \frac{|\mathbf{P}_1|}{|\mathbf{C}_3|} \tag{3.7}$$

is the almost spherical surface first described by Laplace as the sphere of influence. A detailed derivation given by Chobotov [8] and Battin [9] yields for the radius R_i of the sphere of influence, the following expression

$$R_i = \rho \left(\frac{m_3}{m_1} \right)^{2/5} \left(\frac{1}{1 + 3\cos^2 \phi} \right)^{\frac{1}{10}} \tag{3.8}$$

where ϕ is the angle between the vectors $\mathbf{d}$ and $\boldsymbol{\rho}$. It can be readily seen from varying ϕ from $0\,^\circ$ to $90\,^\circ$ that the surface of the sphere of influence is a flattened spheroid with a radius variation of approximately 15% as shown in Fig. 3.1.

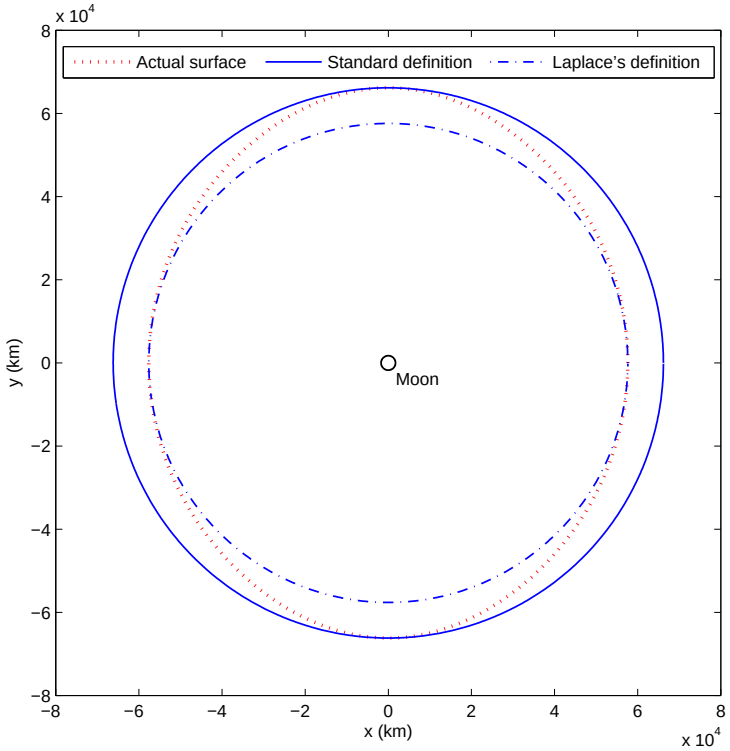

Figure 3.1: Variation in the size of the Sphere of Influence.

When Laplace first derived the radius of this sphere, he used a value of $\phi = 0\,^\circ$.

$$R_i = \rho \left(\frac{m_3^2}{2m_1^2} \right)^{1/5}. \tag{3.9}$$

However, it is generally agreed upon in the literature that the sphere of influence of the planet is defined by the value of the maximum radius of the sphere which occurs when $\phi = 90\,^{\circ}$.

$$R_i = \rho \left(\frac{m_3}{m_1} \right)^{2/5}. \tag{3.10}$$

Of all the different definitions of a gravitational sphere, the sphere of influence, sometimes referred to as the sphere of activity [6] or sphere of action [8], is the most commonly used.

3.3 Hill Sphere

The concept of the Hill sphere, named after 19th century American astronomer George William Hill, was developed upon the principles of the restricted three-body problem. This is a special case of the three-body problem where one of the masses is infinitesimal, such as a spacecraft, so that its motion is affected by the gravitational influences of the other two bodies, but conversely it has no appreciable affect on either of them. Fundamental to the solution of this problem is the expression

$$\dot{x}^2 + \dot{y}^2 + \dot{z}^2 = n^2(x^2 + y^2) + \frac{2Gm_1}{r} + \frac{2Gm_3}{d} - C \tag{3.11}$$

which is known as Jacobi's integral. Here C is a constant of integration, n is the mean motion $\sqrt{G(m_1 + m_3)/\rho^3}$, and the left hand side is the square of the magnitude of the velocity of the infinitesimal mass relative to the rotating reference frame.

If the velocity of the infinitesimal body goes to zero, equation (3.11) reduces to

$$n^2(x^2 + y^2) + \frac{2Gm_1}{r} + \frac{2Gm_3}{d} = C \tag{3.12}$$

where C is uniquely fixed by the initial conditions of position and velocity. For certain values of C, there are inaccessible regions in the rotating frame, as shown by the shaded area in Fig. 3.2. These inaccessible regions, whose boundaries are called zero velocity curves, divide the accessible regions into three regions, two interior and one exterior [10].

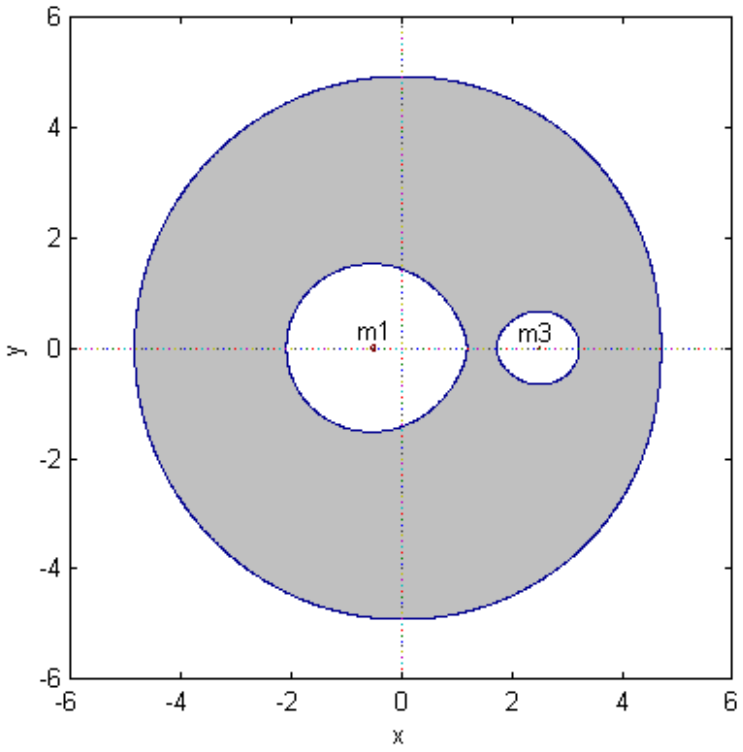

Figure 3.2: Zero velocity curves for a specified value of C.

Since a particle's velocity cannot be imaginary, it holds true that those accessible regions, known historically as Hill's regions, are governed by the inequality $2U > C$ where

$$U = \frac{n^2}{2}(x^2 + y^2) + \frac{Gm_1}{r} + \frac{Gm_3}{d}. \tag{3.13}$$

Thus equation (3.12) is important in that it defines for a specific value of C the boundaries of the regions within which the particle is confined indefinitely. As the value of C decreases, the area of the accessible region grows continually larger, while the forbidden regions shrink gradually smaller until they vanish altogether. The distance to the positions along the rotating x-axis at which the zero velocity curves of the two interior regions first open to each other and to the exterior region can be approximated as

$$R_h = \rho \left(\frac{m_3}{3m_1} \right)^{1/3} \tag{3.14}$$

These points constitute two of the three co-linear Lagrange points, and the given approximation defines the radius of the Hill sphere [11]. For a more comprehensive development of the Jacobi integral and the associated zero velocity curves, the reader is referred to Roy [12] and Battin [9].

3.4 Kislik Sphere

A final concept for the development of a gravitational sphere was presented more recently by Kislik in 1964 [13]. His approach is also based on the principles of the restricted three-body problem and invokes the use of Jacobi's integral. Using the example of a Sun-planet system, he examined the point at which the trajectory of an artificial celestial body changes from rectilinear motion directed radially outward from the planet, to elliptical motion about the sun.

If m_1 and m_2 are the masses of the Sun and planet respectively, the constant of Jacobi's integral at initial time $t = t_0$ can be expressed in unitless quantities as

$$C' = r_0^2 + \frac{2\kappa}{r_{20}} + 2\frac{1-\kappa}{r_{10}} - V_*^2 - r_{20}^2 \tag{3.15}$$

where r_0, r_{10} and r_{20} are the initial distances of the spacecraft from the Sun-planet barycenter, the center of the Sun and the center of the planet respectively, V_* is the magnitude of the absolute velocity of the spacecraft, and κ is the mass ratio $m_2/(m_1 + m_2)$. In the limit for $r_0 \to (1 - \kappa)$, $r_{10} \to 1$ and $r_{20} \to 0$, equation (3.15) reduces to

$$C' = \kappa^2 - 4\kappa + 3 - h \quad \text{where} \quad h = V_*^2 - r_{20}^2. \tag{3.16}$$

The constant of Jacobi's integral which describes the initial part of the elliptical trajectory at some later time t, has the similar form

$$\overline{C} = r^2 + \frac{2\kappa}{r_2} + 2\frac{1-\kappa}{r_1} - V^2 \tag{3.17}$$

where V is the magnitude of the relative velocity of the spacecraft. There exists a point along the trajectory where $\Delta C = \overline{C} - C'$ has a minimum value, and the boundary of the gravitational sphere defined by Kislik passes through this point. The expression he derived for the radius R_k, of this sphere is given by

$$R_k = 1.15\rho \left(\frac{m_3}{m_1}\right)^{1/3}. \tag{3.18}$$

Along with Kislik's original paper, a more detailed discussion of the Kislik sphere can be found in Rauschenbakh *et al.* [5].

A simple expression comparable to the Hill sphere and Kislik sphere can be made by equating the mean motion of the infinitesimal mass m_2 about the secondary body m_3, with the mean motion of m_3 about the primary mass m_1.

$$\sqrt{G(m_2 + m_3)/R^3} = \sqrt{G(m_3 + m_1)/\rho^3}. \tag{3.19}$$

By making the simplifying assumption that $m_1 >> m_3 >> m_2$, m_2 can be neglected from the left hand side of equation (3.19) and m_3 can be neglected from the right hand side. It then becomes a matter of basic algebra to obtain the expression

$$R = \rho \left(\frac{m_3}{m_1} \right)^{1/3}. \tag{3.20}$$

In general, the definition of a sphere of gravitational influence of a particular body can be viewed as the region of space within which it is possible to neglect the gravitational influence of third bodies and assume without great error that any motion within it occurs in a Keplerian orbit [14]. A summarized list of the expressions for each gravitational sphere is provided in Table (3.1) along with the values of the radii of the various gravitational spheres for the Earth-Moon system and the Sun-Earth system. Although there are many different definitions for exactly where the boundary of a gravitational sphere lies, the concept is certainly convenient and widely used, particularly in planning translunar and interplanetary trajectories.

Table 3.1: Radii of various Gravitational Spheres for the Earth-Moon (E-M) and Sun-Earth (S-E) system

Name of Sphere	Expression	E-M (km)	S-E (km)
Sphere of Gravitation 1	$R_{g_1} = \frac{\rho}{1+(m_1/m_3)^{1/2}}$	38,375	258,813
Sphere of Gravitation 2	$R_{g_2} = \rho\sqrt{\frac{m_3}{m_1}}$	42,631	259,262
Sphere of Influence	$R_i = \rho \left(\frac{m_3}{m_1} \right)^{2/5}$	66,182	924,648
Hill Sphere	$R_h = \rho \left(\frac{m_3}{3m_1} \right)^{1/3}$	61,523	1,496,560
Kislik Sphere	$R_k = 1.15\rho \left(\frac{m_3}{m_1} \right)^{1/3}$	102,042	2,482,175

Chapter 4

Chaos

4.1 Historical Perspective

In the late 1950s, a meteorologist at MIT named Edward Lorenz acquired a Royal McBee LGP-30 computer in order to run his weather prediction simulations which incorporated a system of twelve differential equations to model a miniature atmosphere. The computer was the size of a refrigerator, contained 16kB of internal memory and it could calculate at the rate of 60 multiplications per second and print at the speed of six lines of numbers per minute [15]. Such capabilities were extremely impressive for the time.

In 1961 after noticing a particularly interesting sequence, Lorenz decided to re-run the simulation and view it in more detail. However, rather than start the simulation over from the beginning, he simply entered in initial values obtained from the printout of the simulation results. Returning a short time later, he discovered that the sequence he had observed earlier, had evolved along a completely different trajectory. This behavior can be seen in Fig. 4.1 which illustrates a numerical simulation of one variable in the Lorenz system. The curves represent the propagation of initial conditions differing by only 0.0001. At first they appear to coincide, but soon chaotic dynamics leads to independent, widely divergent trajectories.

After some initial investigation, Lorenz realized that the discrepancies lay in the fact that calculations on his computer were performed with a 6-digit precision, whereas the numbers he entered from the printout only contained three significant

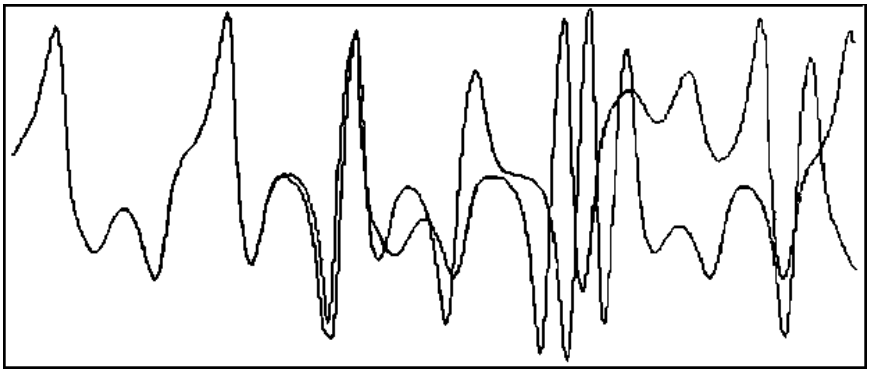

Figure 4.1: Evolution of Lorenz's experiment (Reproduced from [16]).

digits. This observation suggested that there exists, for certain types of systems, a strong sensitivity to initial conditions. Thus, an arbitrarily small perturbation of the trajectory at an initial time t_0, may lead to significantly different behavior at some future time.

Sensitivity to initial conditions is a characteristic of *chaotic* motion, and is popularly known as the *butterfly effect*. The name comes from the title of a paper presented by Edward Lorenz in 1972 [17] to the American Association for the Advancement of Science in Washington, D.C. entitled "Predictability: Does the Flap of a Butterfly's Wings in Brazil set off a Tornado in Texas?" The paper addressed the issue of whether the flapping of a single butterfly's wing produces a tiny change in the state of the atmosphere. Over a period of time, the tiny change can evolve into a significant departure [16].

Although many others, including Hadamard, Poincaré, Birkhoff, Kolmogorov, Cartwright, Littlewood and Smale, had initial insights to chaos theory prior to Lorenz, much of it was under the auspices of ergodic theory. As such, chaos was not truly formalized until the latter part of the 20^{th} century, and despite the fact that Lorenz's 1963 publication [18] was largely ignored for ten years, it is now seen as a prescient beginning to the study of chaos.

4.2 Chaos Theory and Dynamic Systems

A dynamic system is a set of states combined with a *rule* for computing the current values of the states from previous values. Typically, they are categorized as either linear or nonlinear. The only possible behaviors of a linear system are (i) unbounded growth, (ii) decay to equilibrium, or (iii) peridoic oscillation where both (ii) and (iii) represent asymptotically periodic motion. Nonlinear systems, on the other hand, can exhibit a broader class of behaviors including a separate type of motion known as chaos.

Chaos is concerned with the irregular behavior of solutions to deterministic equations of motion and has received much attention from mathematicians and physicists over recent years. The equations must be nonlinear to generate chaotic solutions, but apart from that can be remarkably simple [19]. According to the Poincaré-Bendixson Theorem, chaotic behavior can only arise in *continuous* dynamical systems whose phase space has three or more dimensions. However the theorem does not apply to *discrete* dynamical systems, where chaotic behavior can arise in two or even one dimensional systems.

As mentioned previously, a characteristic feature of chaotic motion is that any tiny errors in current knowledge makes accurate prediction into the future very difficult to obtain. It is not however the same as stochastic motion, which occurs in the case where even exact knowledge of the current state does not allow prediction of future behavior. The presence of chaotic motion in models of nature can be significant, since in any physical system it is almost impossible to obtain perfectly precise knowledge of current conditions.

The rule mentioned above is sometimes referred to as a *map* if it is used to denote some function f whose domain space is equal to the range space. A particular one

dimensional map, called the Logistic map, is a convenient example of how a very simple, nonlinear dynamical equation can exhibit complex and chaotic motion. It is based on the logistic growth model equation

$$f(x) = ax(1 - x) \tag{4.1}$$

first created by Pierre François Verhulst in 1845 to describe population growth and decay. For the equation to possess non-trivial dynamical behavior, the growth rate a, and the state variable x, must respectively remain on the intervals $1 < a < 4$ and $0 < x < 1$. If $a < 1$, all trajectories are attracted towards $x = 0$, whereas for the case where $a > 4$ or x exceeds unity, the system diverges towards $-\infty$ [20]. Fig. 4.2, known as a bifurcation diagram, shows the long term possible values of x plotted against various values of a starting at $a = 2.4$.

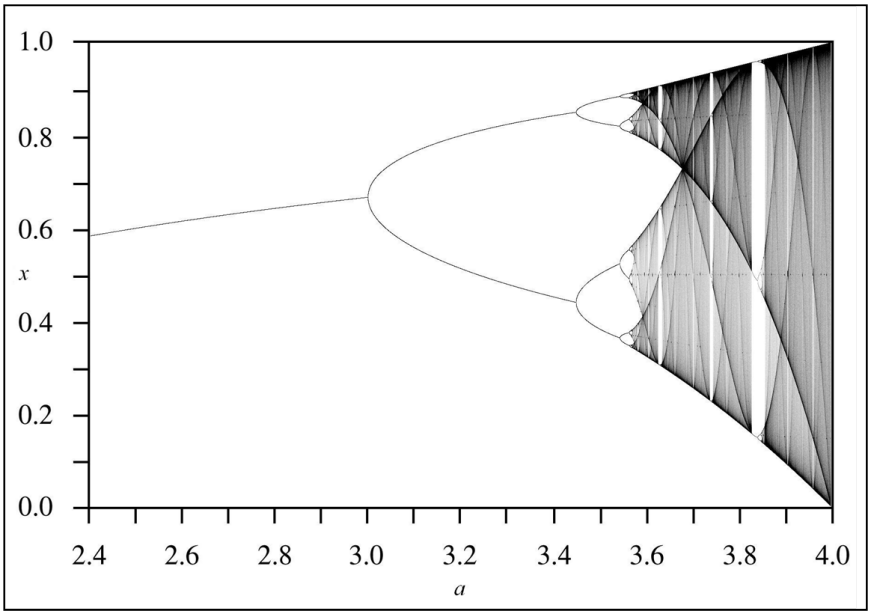

Figure 4.2: A bifurcation diagram for the Logistic map (reproduced from [21]).

Some key features to observe from this diagram include the period doubling at approximately $a = 3$, the start of the period-four trajectory at $a \approx 3.45$ and the

beginning of chaotic motion at around $a = 3.57$. It is also interesting to note the *windows* that appear, particularly the prominent three-period window in the region of $a = 3.84$.

One of the most famous maps is the 3-dimensional Lorenz attractor which shows how the state of a dynamical system can evolve over time in a complex, non-repeating pattern. It is governed by the ordinary differential equations (ODE's) used in Lorenz's simplified model of the atmosphere, and from certain perspectives, has the coincidental appearance of a *butterfly* (see Fig. 4.3). Since the dynamics on it are chaotic, it is referred to as a *strange* attractor.

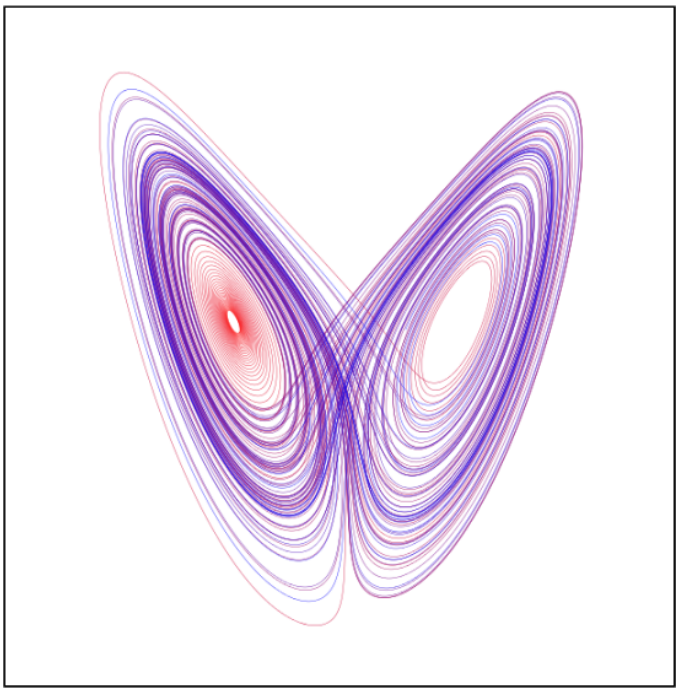

Figure 4.3: The Lorenz Attractor (reproduced from [22]).

4.3 Lyapunov Exponents

Various methods have been devised over the years to make quantitative statements about the exponential divergence of infinitesimally close trajectories in chaotic

systems. One such method, named after the Russian mathematician Aleksandr Lyapunov, incorporates the use of special constants called Lyapunov exponents. A closely related value is the Lyapunov number, and both can be viewed as the averaged rate of divergence (or convergence) of nearby points along the trajectory [23].

More formally, let f be a smooth map of the real line $\mathbb{R}$. The Lyapunov number $L(x_1)$ of the trajectory $\{ x_1, x_2, x_3, ... \}$ is defined as [15]

$$L(x_1) = \lim_{n\to\infty} (|f'(x_1)|...|f'(x_n)|)^{\frac{1}{n}} \tag{4.2}$$

if this limit exists. The Lyapunov exponent $\lambda(x_1)$ is defined as

$$\lambda(x_1) = \lim_{n\to\infty} \frac{1}{n}[\ln|f'(x_1)| + ... + \ln|f'(x_n)|] \tag{4.3}$$

if this limit exists. Notice that $\lambda = \ln L$, and therefore exists if and only if L exists and is nonzero. With this definition of the Lyapunov exponent firmly set, it is now possible to formally define chaotic motion. Once again, let f be a smooth map of the real line $\mathbb{R}$. The trajectory $\{ x_1, x_2, x_3, ... \}$ generated by f is chaotic if all the following conditions are satisfied:

1) it is bounded,

2) it is not asymptotically periodic,

3) the Lyapunov exponent $\lambda(x_1)$ is greater than zero.

A simple example of calculating $L(x_1)$ and $\lambda(x_1)$ can be illustrated by examining the following system known as a tent map

$$T(x) = \begin{cases} 2x, & \text{if } x \leq 1/2 \\ 2(1-x), & \text{if } x \geq 1/2. \end{cases} \tag{4.4}$$

Differentiating with respect to x yields

$$T'(x) = \begin{cases} 2, & \text{if } x \leq 1/2 \\ -2, & \text{if } x \geq 1/2. \end{cases} \tag{4.5}$$

Then for any trajectory,

$$L(x_1) = \lim_{n\to\infty} (2^n)^{\frac{1}{n}} = 2 \tag{4.6}$$

regardless of initial condition. Also, $\lambda(x_1) = \ln(2) = 0.6931$.

It is relatively easy to obtain an analytical solution for the Lyapunov exponent of the tent map. However, for most dynamical systems, especially continuous systems, the solution is not so easy to obtain analytically and must therefore be found numerically. One such numerical method is known as Wolf's algorithm. Consider two trajectories initially separated by d_0. After n iterations they are separated by d_n. This separation can be expressed as

$$d_n \approx d_0 e^{\lambda n}, \tag{4.7}$$

which can then be solved for λ as follows

$$\frac{d_n}{d_0} \approx e^{\lambda n}$$
$$\ln\left[\frac{d_n}{d_0}\right] \approx \lambda n$$
$$\lambda \approx \lim_{n\to\infty} \frac{1}{n} \ln\left[\frac{d_n}{d_0}\right].$$

Now consider a higher dimensional system on $\mathbb{R}^m$ where m is the number of elements in the state vector. For an initial condition $\mathbf{x}_0$, there exists a neighboring initial condition, namely $\mathbf{x}_0 + \Delta\mathbf{x}$, in any arbitrary direction which belongs to a hypersphere about $\mathbf{x}_0$. The rate of separation between the two initial conditions over time can be different for different orientations of the initial separation vector, $\mathbf{r}$, thus transforming the hypersphere into a hyperellipse as illustrated in Fig. 4.4. A system will have as many Lyapunov exponents as the dimension of the state space, as can be seen in the following definition.

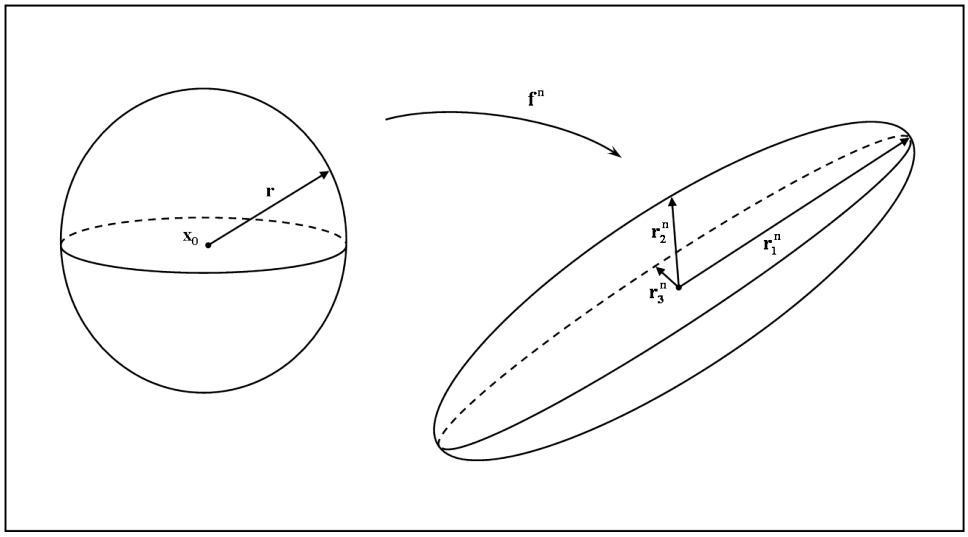

Figure 4.4: Evolution of an initial infinitesimal hypersphere.

Let $\mathbf{f}$ be a smooth map on $\mathbb{R}^m$, and for $k = 1, ..., m$, let r_k^n be the length of the kth longest orthogonal axis of the ellipsoid. If $r = |\Delta \mathbf{x}|$, the kth Lyapunov number of $\mathbf{x_0}$ is defined by

$$L_k = \lim_{n \to \infty} \lim_{r \to 0} \left(\frac{r_k^n}{r} \right)^{\frac{1}{n}} \tag{4.8}$$

if this limit exists. The kth Lyapunov exponent is $\lambda_k = \ln L_k$. Also by definition, $L_1 \geq L_2 \geq ... \geq L_m$ and $\lambda_1 \geq \lambda_2 \geq ... \geq \lambda_m$.

The largest such exponent is of most interest because it determines the predictability of a dynamical system. It measures the average rate of exponential divergence of nearby trajectories of the chaotic mapping along the direction of greatest expansion. A positive exponent will suggest that trajectories tend to separate rather than to remain parallel or close to one another, indicative of chaotic motion [24]. For various values of λ, the trajectory of a dynamical system exhibits the following behaviors.

$\lambda < 0$: The trajectory attracts to a stable fixed point or stable periodic orbit. Negative Lyapunov exponents are characteristic of systems that exhibit asymptotic stability. The more negative the exponent, the greater the stability, and the system heads towards its equilibrium point as quickly as possible.

$\lambda = 0$: A Lyapunov exponent of zero indicates that the system is in some sort of steady state mode. Such systems exhibit Lyapunov stability.

$\lambda > 0$: The trajectory is unstable and chaotic. Nearby points, no matter how close, will diverge to any arbitrary separation. The greater the value of λ, the more chaotic the motion, thus the stochastic model is characterized by the case where $\lambda \to \infty$.

4.4 State Transition Matrix

Up to this point, discrete systems have been discussed. Now, the chaotic motion of continuous systems will be considered. As illustrated in equation (4.8), the value of the Lyapunov number can be calculated by having an explicit knowledge of the ratio of the axes of the hyperellipsoid to the radius of the initial hypersphere. One method for evaluating this ratio invokes the use of the *state transition matrix*, which is a matrix of partial derivatives which maps deviations in the state vector from one time to another [25].

Consider a dynamical system governed by the first-order differential equation and a given initial condition

$$\dot{\mathbf{x}} = \mathbf{f}(\mathbf{x}, t) \qquad \mathbf{x}(t_0) = \mathbf{x}_0 \tag{4.9}$$

and define the state transition matrix as

$$\mathbf{\Phi} \equiv \frac{\partial \mathbf{x}(t)}{\partial \mathbf{x_0}} \tag{4.10}$$

where $\mathbf{x}(t)$ is the state vector at some future time t. It is easily observed that evaluating $\mathbf{\Phi}$ at the initial time t_0 yields the identity matrix. Then by taking the time derivative of $\mathbf{\Phi}$, the following sequence of expressions is obtained

$$\begin{aligned}
\dot{\mathbf{\Phi}} &= \frac{d}{dt}\left(\frac{\partial \mathbf{x}(t)}{\partial \mathbf{x_0}}\right) \\
&= \frac{\partial}{\partial \mathbf{x_0}}\left(\frac{d\mathbf{x}}{dt}\right) \\
&= \frac{\partial}{\partial \mathbf{x_0}}(\mathbf{f}(\mathbf{x}, t)) \\
&= \frac{\partial \mathbf{f}}{\partial \mathbf{x}}\frac{\partial \mathbf{x}}{\partial \mathbf{x_0}}
\end{aligned}$$

$$\dot{\mathbf{\Phi}} = \mathbf{A}\mathbf{\Phi} \qquad \text{where} \qquad \mathbf{A} = \frac{\partial \mathbf{f}}{\partial \mathbf{x}} \tag{4.11}$$

By using the differential equations which describe the system, $\mathbf{A}$ can be calculated and used to obtain a solution for $\mathbf{\Phi}$. Then, if $\delta\mathbf{x_0}$ represents a small variation from the initial condition, the deviation from the nominal trajectory at some later time, t, can be expressed as $\delta\mathbf{x}(t) = \mathbf{\Phi}\delta\mathbf{x_0}$. The magnitude of this deviation can then be calculated as $|\delta\mathbf{x}| = \sqrt{\delta\mathbf{x_0}^T\mathbf{\Phi}^T\mathbf{\Phi}\delta\mathbf{x_0}}$. Finally, by dividing through by the magnitude of the variation in the initial condition

$$\frac{|\delta\mathbf{x}|}{|\delta\mathbf{x_0}|} = \frac{\sqrt{\delta\mathbf{x_0}^T\mathbf{\Phi}^T\mathbf{\Phi}\delta\mathbf{x_0}}}{\sqrt{\delta\mathbf{x_0}^T\delta\mathbf{x_0}}} = \frac{\sqrt{D_k\delta\mathbf{x_0}^T\delta\mathbf{x_0}}}{\sqrt{\delta\mathbf{x_0}^T\delta\mathbf{x_0}}} = \sqrt{D_k} \tag{4.12}$$

it can be seen that the square roots of the m eigenvalues, D_k, of the symmetric matrix $\mathbf{\Phi}^T\mathbf{\Phi}$ give the ratio of the axes of the hyperellipse to the radius of the initial hypersphere. This value of course can then be used directly in equation (4.8) to compute the associated Lyapunov exponents, remembering that the exponent of greatest interest is the largest exponent λ_1.

Chapter 5

Simulation Model

The motion of a spacecraft in cislunar space is governed primarily by the gravitational fields of the Earth and the Moon. The effects of solar gravity and the perturbations arising from the nonspherical shape of the attracting bodies are important in a final analysis but are neglected in obtaining the trajectories for this simulation.

In this study the positions of the spacecraft, Earth, and Moon are described by the relative position vectors as shown in Fig. 5.1, where $\mathbf{r}$ is the position of the spacecraft relative to the Earth, $\mathbf{d}$ is the position of the spacecraft relative to the Moon, and $\boldsymbol{\rho}$ is the position of the Moon relative to the Earth. For simplifying purposes, the dynamical model used is assumed to be coplanar. The mass of the Earth is m_e, the mass of the Moon is m_m, and the mass of the spacecraft is m_s.

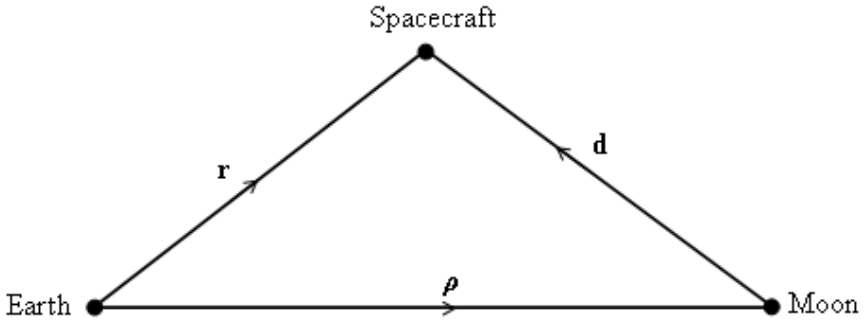

Figure 5.1: Position vectors between the vehicle, Earth, and Moon.

The translunar trajectories studied in this work can be considered solutions to the three-body problem. As described in Chapter 2, the relative motion of the vehicle can be described with respect to either the Earth or the Moon. This gives

rise to alternative sets of equations of motion in either an Earth-centered (EC) or Moon-centered (MC) reference frame. The total acceleration in either representation contains a central-body acceleration and a perturbative term. By the condition that $m_s << m_m << m_e$, it is a reasonable simplification to neglect m_s. Then by introducing the standard gravitational parameters, μ_e=Gm_e and μ_m=Gm_m, equations (2.17) and (2.18) can be re-written in a slightly simplified form. Thus, the equation of motion in the EC frame becomes

$$\frac{d^2\mathbf{r}}{dt^2} + \frac{\mu_e}{r^3}\mathbf{r} = -\mu_m \left(\frac{\mathbf{d}}{d^3} + \frac{\boldsymbol{\rho}}{\rho^3} \right) \tag{5.1}$$

where the Earth is the central body and the Moon causes a perturbative acceleration. The equation of motion in the MC frame is similar, however, the Moon is now treated as the central body and the Earth causes the perturbative acceleration.

$$\frac{d^2\mathbf{d}}{dt^2} + \frac{\mu_m}{d^3}\mathbf{d} = -\mu_e \left(\frac{\mathbf{r}}{r^3} - \frac{\boldsymbol{\rho}}{\rho^3} \right). \tag{5.2}$$

Since the eccentricity of the Moon's orbit is very small, $e = 0.0549$, the trajectory of the Moon was modeled as a circular orbit using the following expression.

$$\boldsymbol{\rho} = \rho \begin{bmatrix} \cos(\omega_m t) \\ \sin(\omega_m t) \end{bmatrix}. \tag{5.3}$$

Here, the value of the Moon's angular velocity, $\omega_m = 2\pi/T_m$, was obtained using Kepler's third law of planetary motion

$$\left(\frac{T_m}{2\pi} \right)^2 = \frac{\rho^3}{G(m_e + m_m)} \tag{5.4}$$

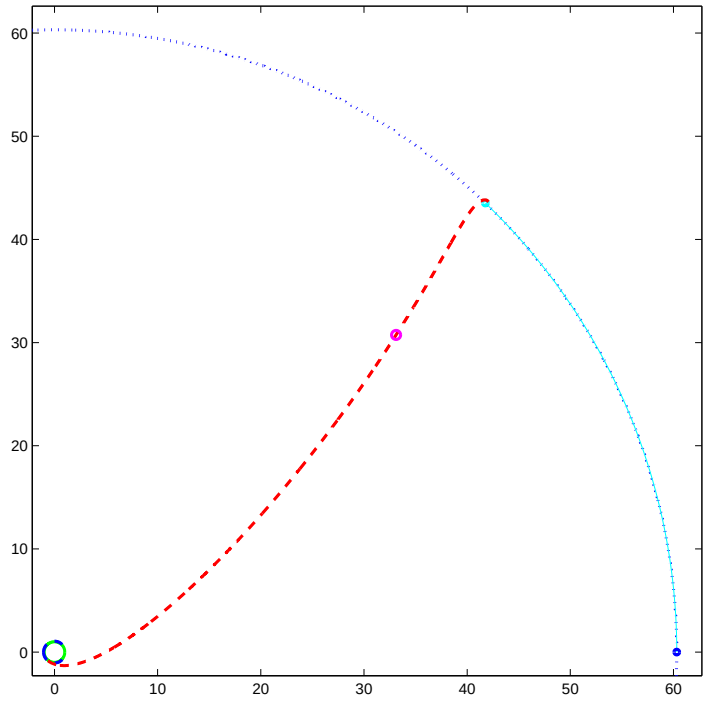

Figure 5.2: Diagram of the translunar trajectory.

to solve for T_m, and a value of $\rho = 384,400$ km was used as the semi-major axis of the Moon's orbit.

A nominal trip time of 3.5 days was chosen for the trajectory, and an integration time step of 20 secs was used for all simulations. The vehicle trajectory in the EC and MC reference frames were simulated by numerical integration of equations (5.1) and (5.2) respectively. The Moon position was updated every half time step to maintain consistency with the the fourth-order Runge-Kutta (RK4) integration scheme (see Appendix A). This RK4 scheme was used to perform all integrations in this study, and simulation accuracy was improved significantly by updating the ephemerides at each intermediate time step.

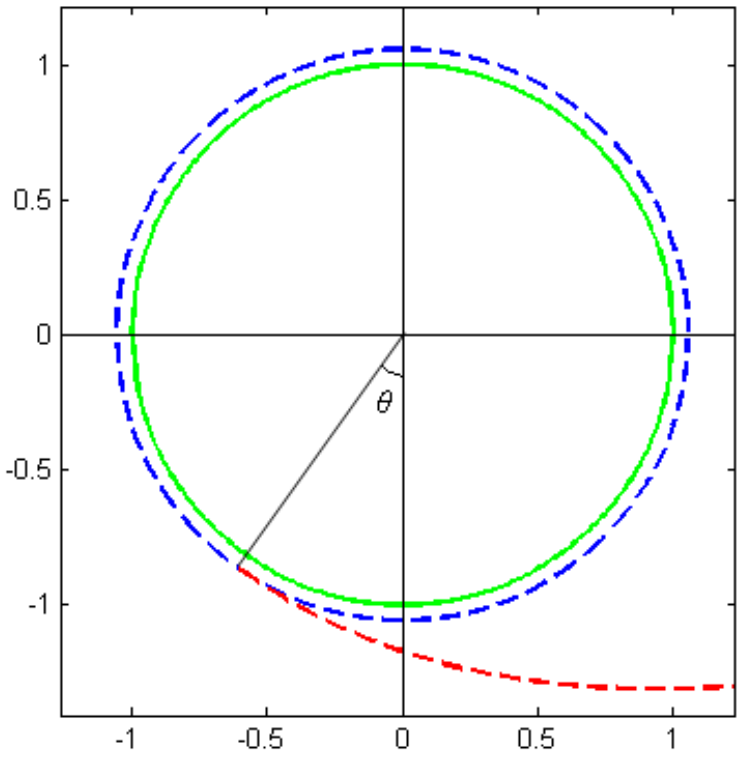

Figure 5.3: Plot of the Earth, low Earth orbit, point of Δv, and initial trajectory.

The starting location of the Moon was set at a distance ρ directed out from the Earth along the positive x-axis as shown in Fig. 5.2. Altitudes of h = 359,750 m to 360,250 m in 50 m increments were chosen for the initial low Earth orbit (LEO), and a Δv of 3102.13 m/s was applied at varying angles from $\theta = -36.970\,^\circ$ to $-36.906\,^\circ$ in increments of $0.008\,^\circ$ from the negative y-axis. A magnified view of the initial part of the trajectory is illustrated in Fig. 5.3, and for convenience, table 5.1 lists the physical parameters used in this simulation.

There are two main types of error invoked in this particular simulation, namely discretization and round-off errors. Whereas iterative error may be significant in other simulations, it was not the case in this study. In the equations of motion, calculation of the perturbative acceleration can include larger amounts of round-off error than the central-body acceleration. This is because, for certain configurations

Table 5.1: Physical Parameters of the Simulation Model

Parameter	Value	Units
t_0	0	secs
Δt	20	secs
t_f	3.5	days
μ_m	4.90266 x 10^{12}	m^3/s^2
μ_e	3.98600436 x 10^{14}	m^3/s^2
r_e	6,372.797	km
Δv	3,102.13	m/s
θ	-36.970 to -36.906	degrees
h	359.750 to 360.250	km
ρ	384,400	km

of the bodies, calculation of the perturbative acceleration can require subtraction of similar numbers. Considering the EC representation, when the spacecraft is close to the Earth, summing $\mathbf{d}/d^3$ and $\boldsymbol{\rho}/\rho^3$ can require differencing similar numbers. When the spacecraft is close to the Moon, calculating $\mathbf{d} = \mathbf{r} - \boldsymbol{\rho}$ requires differencing similar numbers. One method of circumventing the former difficulty is by defining two new variables, q and f

$$q = \frac{\mathbf{r} \cdot (\mathbf{r} - 2\boldsymbol{\rho})}{\boldsymbol{\rho} \cdot \boldsymbol{\rho}} \tag{5.5}$$

$$f = \frac{3q + 3q^2 + q^3}{1 + (1+q)^{3/2}}. \tag{5.6}$$

Now equation (5.1) can be expressed using f as follows [9]

$$\frac{d^2\mathbf{r}}{dt^2} = \frac{-\mu_e}{r^3}\mathbf{r} - \frac{\mu_m}{|\mathbf{r} - \boldsymbol{\rho}|^3}(\mathbf{r} + f\boldsymbol{\rho}). \tag{5.7}$$

In order to investigate the effect of coordinate choice on round-off error, a MATLAB simulation was created that allowed switching at various points between the

EC and MC models. This simulation was implemented with single precision computations. To estimate the amount of roundoff error, the results were compared to a "truth" simulation which was computed using double precision and the entire trajectory was propagated in EC. The root-mean-square over the entire trajectory of the norm of the position errors between the single and double precision calculations was chosen for the error estimate.

In MATLAB, a floating-point number handled in double precision format uses 64 bits (8 bytes) of memory storage based on IEEE Standard 754. Double-precision variables accurately represent values to approximately fifteen decimal places. The lower 32-bit single-precision variables represent data to about seven decimal places.

Chapter 4 introduced the idea that in modern dynamic-system theory, the propagation of small initial errors in numerical simulations can be related to chaotic motion. The differences in roundoff errors between the EC and MC frames can be related to the Lyapunov exponents of the two representations. The loss of precision due to taking the difference of similar numbers is in some sense equivalent to high sensitivity to small perturbations, a characteristic of chaotic motion.

For the EC reference frame, the Lyapunov exponents were calculated as follows. Since $\mathbf{x} = [\mathbf{r}\ \dot{\mathbf{r}}]^T$, then by equation (4.9)

$$\dot{\mathbf{x}} = \begin{bmatrix} \dot{\mathbf{r}} \\ \ddot{\mathbf{r}} \end{bmatrix} = \mathbf{f}(\mathbf{x}, t). \tag{5.8}$$

Then from equation (4.11),

$$\mathbf{A} = \frac{\partial \mathbf{f}}{\partial \mathbf{x}} = \begin{bmatrix} \frac{\partial \dot{\mathbf{r}}}{\partial \mathbf{r}} & \frac{\partial \dot{\mathbf{r}}}{\partial \dot{\mathbf{r}}} \\ \frac{\partial \ddot{\mathbf{r}}}{\partial \mathbf{r}} & \frac{\partial \ddot{\mathbf{r}}}{\partial \dot{\mathbf{r}}} \end{bmatrix} = \begin{bmatrix} \mathbf{0} & \mathbf{I} \\ \mathbf{G} & \mathbf{0} \end{bmatrix} \tag{5.9}$$

where

$$\mathbf{G} = \begin{bmatrix} \frac{\partial \ddot{r}_x}{\partial r_x} & \frac{\partial \ddot{r}_x}{\partial r_y} \\ \frac{\partial \ddot{r}_y}{\partial r_x} & \frac{\partial \ddot{r}_y}{\partial r_y} \end{bmatrix}. \tag{5.10}$$

If $\ddot{r}_x$ and $\ddot{r}_y$ are given respectively as

$$\ddot{r}_x = \frac{-\mu_1 r_x}{(r_x^2 + r_y^2)^{3/2}} - \mu_m \left[\frac{r_x - \rho_x}{[(r_x - \rho_x)^2 + (r_y - \rho_y)^2]^{3/2}} + \frac{\rho_x}{(\rho_x^2 + \rho_y^2)^{3/2}} \right] \tag{5.11}$$

$$\ddot{r}_y = \frac{-\mu_1 r_x}{(r_x^2 + r_y^2)^{3/2}} - \mu_m \left[\frac{r_y - \rho_y}{[(r_x - \rho_x)^2 + (r_y - \rho_y)^2]^{3/2}} + \frac{\rho_y}{(\rho_x^2 + \rho_y^2)^{3/2}} \right] \tag{5.12}$$

then

$$G_{11} = \frac{-\mu_e}{||\mathbf{r}||^3} + \frac{3\mu_e r_x^2}{||\mathbf{r}||^5} - \frac{\mu_m}{||\mathbf{r} - \boldsymbol{\rho}||^3} + \frac{3\mu_m (r_x - \rho_x)^2}{||\mathbf{r} - \boldsymbol{\rho}||^5} \tag{5.13}$$

$$G_{12} = \frac{3\mu_e r_x r_y}{||\mathbf{r}||^5} + \frac{3\mu_m (r_x - \rho_x)(r_y - \rho_y)}{||\mathbf{r} - \boldsymbol{\rho}||^5} \tag{5.14}$$

$$G_{21} = G_{12} \tag{5.15}$$

$$G_{21} = \frac{-\mu_e}{||\mathbf{r}||^3} + \frac{3\mu_e r_y^2}{||\mathbf{r}||^5} - \frac{\mu_m}{||\mathbf{r} - \boldsymbol{\rho}||^3} + \frac{3\mu_m (r_y - \rho_y)^2}{||\mathbf{r} - \boldsymbol{\rho}||^5}. \tag{5.16}$$

Using $\mathbf{A}$ to integrate $\mathbf{\Phi}$, and finding the eigenvalues, D, of the matrix $\mathbf{\Phi}^T \mathbf{\Phi}$, Lyapunov exponents were computed as

$$\lambda = \ln \sqrt{D} \tag{5.17}$$

Chapter 6

Results

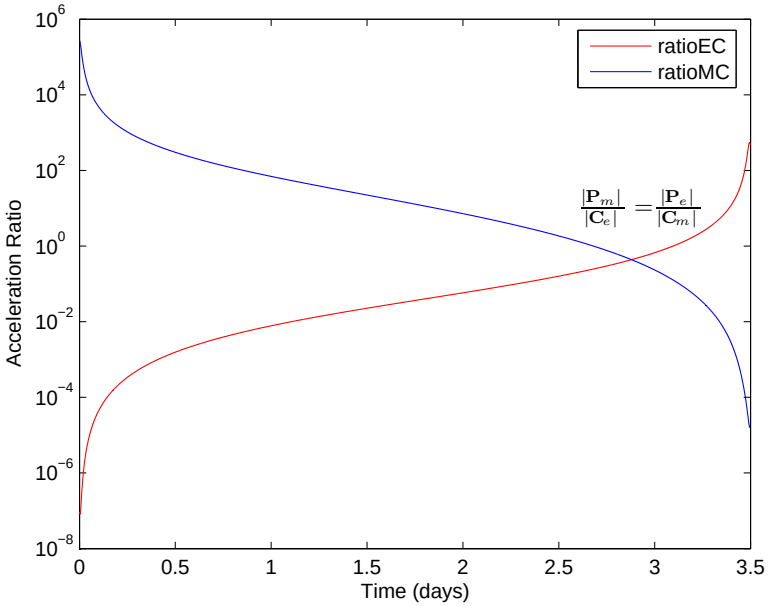

Figure 6.1: Ratio of perturbative to central-body accelerations.

Figure 6.1 presents the ratios of perturbative to central accelerations for EC and MC frames. The ratios clearly illustrate that the gravitational influence of the Earth dominates the trajectory at first, but as the spacecraft approaches the Moon, the gravitational pull of the Moon gradually becomes more dominant. Upon close examination, it is observed that the two curves intersect at $t \approx 2.88$ days which corresponds to a distance from the Moon of approximately 59,400 km.

To examine the effect of coordinate choice on round-off error, the root-sum-squared (RSS) position errors, δ, between single and double precision simulations

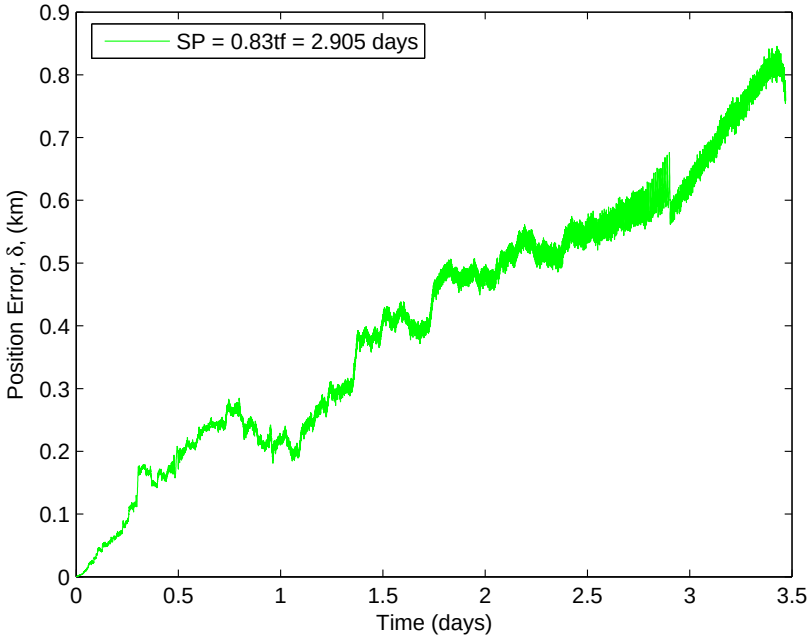

Figure 6.2: Plot of the RSS position error.

were calculated at each time step. These values, which represent the magnitude of the position differences, were obtained for the entire trajectory and plotted with respect to time. Fig. 6.2 illustrates how the position error grows over time for the case where $h = 360$ km, $\theta = -36.930\,^{\circ}$ and where the reference frame is switched from EC to MC at $t = 2.905$ days. It is particularly noticeable that there is a distinct change in the error behavior at the switch point time, proving that a careful selection of the time at which to switch reference frames can affect the round-off error and improve the simulation accuracy.

Figure 6.3 shows sample results for the round-off error between single and double precision calculations using several different switch points. These results clearly indicate that switching coordinates either very early or very late in the trajectory introduces large round-off errors. As mentioned previously, these errors can be mitigated by selecting a more optimal point at which to switch from EC to MC. For this

study, the switch point time was expressed as a percentage of the final time t_f. By plotting the RSS errors for ninety nine switch points, it was observed that switching at $t = 2.905$ days produces a particularly low position error. This corresponds to a distance from the Moon of approximately 57,200 km.

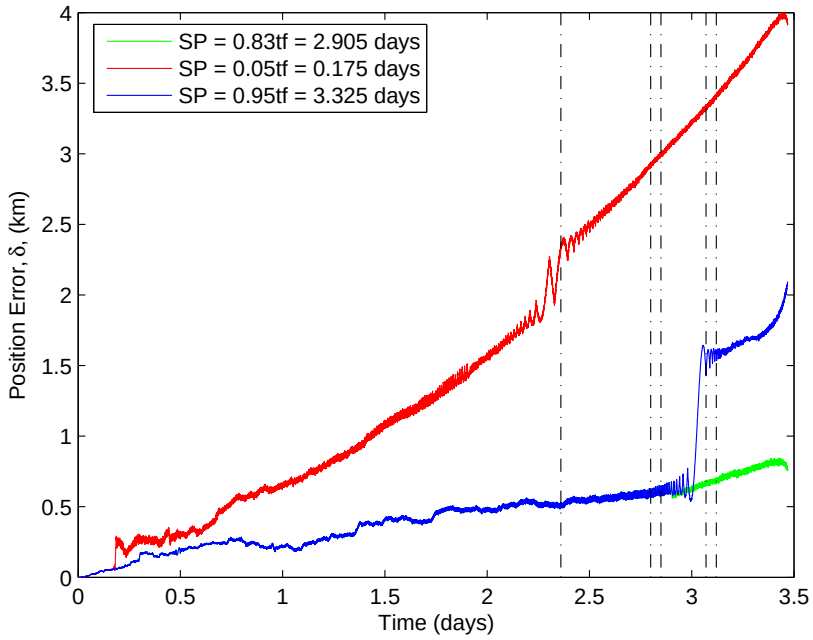

Figure 6.3: RSS position error for three switch point times.

To fully characterize this behavior a range of switch points was investigated, and each switch point was tested for a family of initial conditions. The average error of the plot shown in Fig. 6.2 can be quantified by finding the root-mean-square (RMS) error, ϵ_{rms}, over the entire trajectory as determined from the following expression

$$\epsilon_{\text{rms}} = \sqrt{\frac{\delta_0^2 + \delta_1^2 + \delta_2^2 +, ..., +\delta_n^2}{n}} = \sqrt{\frac{1}{n}\sum_{i=0}^{n} \delta_i^2} \tag{6.1}$$

where $n = t_f/\Delta t$. The RMS errors for ninety nine switch points were then calculated for 121 different sets of initial conditions. The initial conditions investigated were

taken from a combination of the various values for h and θ as described in Chapter 5. Figure 6.4 shows the maximum, minimum, and average RMS values for all initial conditions at each switch point. Although the RMS values begin high, they quickly approach a steady value for later switch point times. Note that the maximum RMS value is less than 20 km.

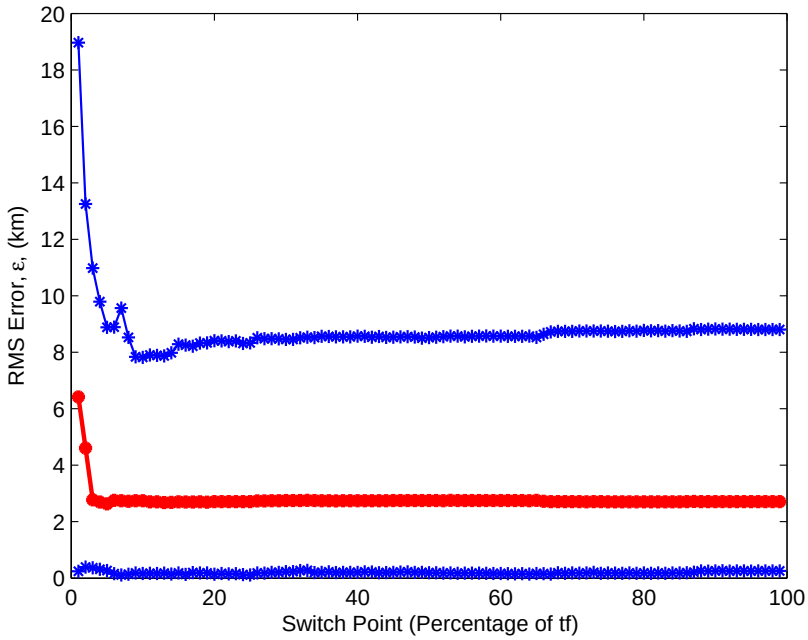

Figure 6.4: Plot of the Maximum, Minimum and Average RMS values

A magnified plot of the average RMS values is shown in Fig. 6.5. Although the lowest average RMS values are obtained be switching reference frames early in the trajectory, certain initial conditions can still induce much higher round-off errors. Therefore, the two points of main interest in the plot appear at switch point times of approximately 67.5% and 85% of t_f. The first point corresponds to a time of 2.3625 days and a distance from the Moon of 102,300 km. Switching from EC to MC at this time produces a sharp reduction in the average RMS value indicative of greater simulation accuracy. The second later point occurs at 2.975 days and a distance from

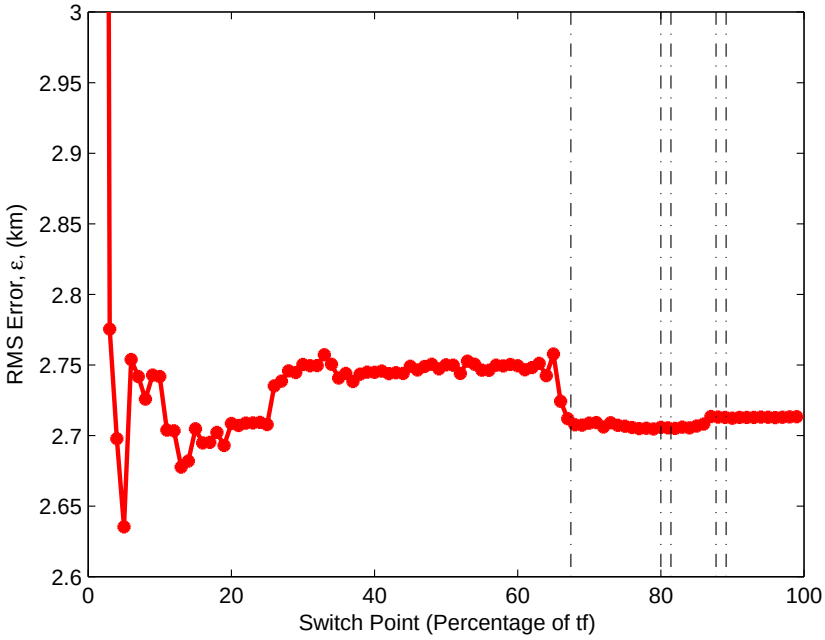

Figure 6.5: Magnified Plot of the Average RMS values

the Moon of 51,200 km. Figure 6.5 shows a very slight increase in RMS error at this point.

It was also necessary to determine if the results in this study were representative of a wide range of initial conditions. To investigate this issue, a switch point time of 1.75 days ($0.5t_f$) was chosen. The average value of the RMS error at that particular switch point was then calculated for varying numbers of simulation trials from 1 to 121, where a simulation trial is defined as a simulation with a specific set of initial conditions. Figure 6.6 shows the results of this investigation. It is evident that by examining less than twenty sets of initial conditions, there is a lot of variance in the results. However, after approximately eighty simulation trials, the average value has converged to a fairly steady value. It can therefore safely be assumed that an investigation of anymore than eighty sets of initial conditions will essentially produce a negligible change in the results.

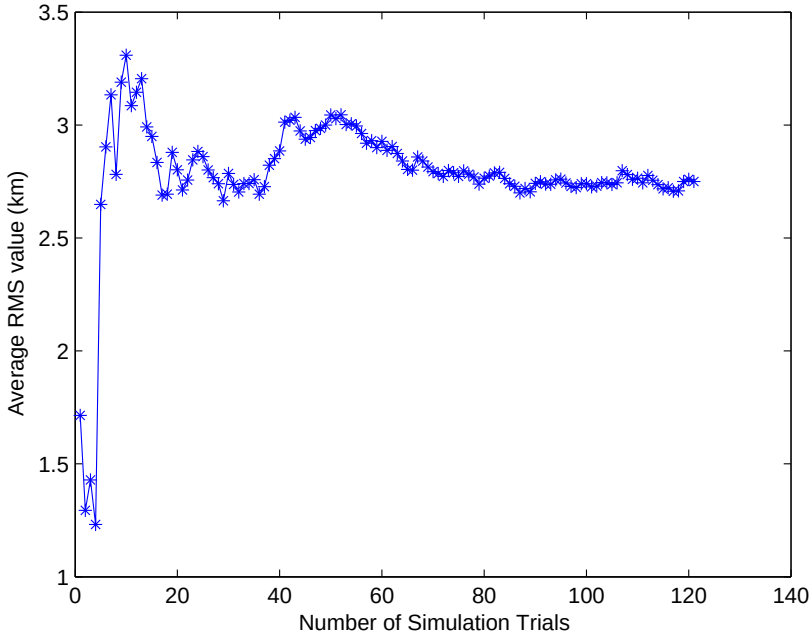

Figure 6.6: Plot to show if simulation results are representative of many initial conditions.

Finally, Fig. 6.7 displays the Lyapunov exponents for the translunar trajectory over one hour intervals. Since the values of the exponents are greater than zero throughout the entire trajectory, it can be asserted that the motion is always chaotic. It is also evident, however, that the values of λ are greater while the spacecraft is in close proximity to the Earth or to the Moon. This suggests that the trajectory is more chaotic during the initial and final stages of the journey.

Table 6.1: Radii of various Gravitational Spheres and Corresponding Switch Point Times

Sphere	Radius (km)	Switch Point (Days)
R_{g_1}	38,375	3.12
R_{g_2}	42,631	3.07
R_h	61,523	2.85
R_i	66,182	2.80
R_k	102,042	2.36

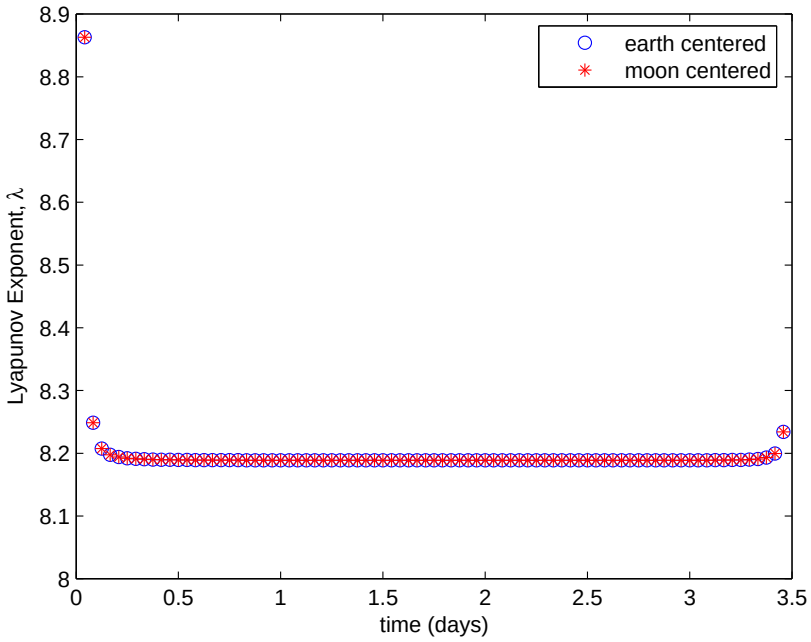

Figure 6.7: Plot of the Lyapunov Exponents for a translunar trajectory.

A summary of the radii of the five gravitational spheres is shown in Table 6.1 along with the corresponding switch point times. Note that the spacecraft enters the Kislik sphere after approximately 2.36 days. This corresponds very well to the sharp decline in the plot shown in Fig. 6.5. Both the Hill sphere and the sphere of influence boundaries occur before the slight rise in the RMS error occurs at 2.975 days. Also, the range of the spacecraft from the Earth and from the Moon is shown in Fig. 6.8. This plot indicates that the spacecraft is equidistant from the Moon and the Earth after approximately 1.062 days.

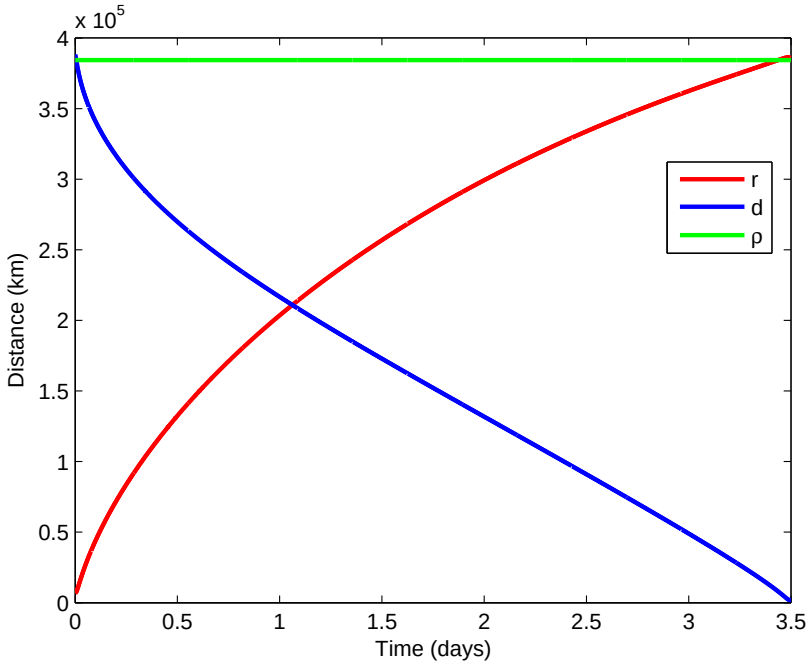

Figure 6.8: Plot of the Spacecraft Range from the Earth and Moon

Chapter 7

Discussion

7.1 Conclusion

In the simulation of translunar trajectories, the vehicle motion can be described in either an EC or MC frame. These coordinate choices have significant impact on the amount of round off error in the simulation. It was shown that the switching from EC to MC coordinates at an appropriate point along the trajectory can minimize precision loss caused by this round off error. The preferred switch point is correlated with the historical concepts of the various gravitational spheres.

The accuracy was significantly improved (regardless of integration frame) if the Moon's ephemerides were updated at each intermediate integration time step. This is due to the fourth-order Runge-Kutta integration scheme used as described in Chapter 5.

From the results presented in Chapter 6, the magnitude of the position difference, induced by round-off errors, ranged from less than 1 km to over 4 km depending of the choice of switch time. Of course, part of the reason for these large magnitudes was the use of single-precision calculations. On the scale of the solar system, these error values might be considered to be very small. In terms of an accurate simulation however, errors of more than a few meters could be viewed as significant. The results obtained in this work indicated a large reduction in accuracy if coordinate switching is used in the first 10% of the trajectory. Fortunately, the results also indicated

that after this initial period, coordinate switching can be performed without large sensitivity to the particular switch point.

Finally, it was distinctly shown that the translunar trajectories investigated in this simulation exhibit chaotic motion. As a result, there is a very apparent sensitivity of the trajectory to initial conditions.

7.2 Future Work

Future work may further investigate other sources of numerical error in translunar trajectory simulations. By decreasing the time step of the integration routine and increasing the amount of precision used in the simulation, the discretization and round-off errors could be respectively reduced. Making both these revisions however would lead to the obvious disadvantage of a significant increase in the simulation runtime. Richardson extrapolation can be used to estimate discretization error, and the method of nearby problems can be used to characterize the total numerical error. It may also be insightful to obtain more data by examining a wider variety of initial conditions. This might include varying Δv, as well as extending the range of h and θ_0 values used. A more detailed analysis of the Lyapunov exponents, and the similarities of the simulated lunar trajectories to chaos theory could also be be undertaken.

Bibliography

[1] Turnball, H., *The Great Mathematicians*, Methuen & Co Ltd, London, 1951.

[2] Gillies, G. T. *The Newtonian Gravitational Constant: Recent Measurements and Related Studies*, Rep. Prog. Phys. 60, 1997, pp. 151-225.

[3] Cvitanović, P. Artuso, R. Mainieri, R. Tanner, G., and Vattay, G., *Chaos: Classical and Quantum*, Niels Bohr Institute, Copenhagen, 2005, URL: `http://chaosbook.dk/postscript.shtml` [cited 30 March 08].

[4] Gurzadyan, G. A., *Theory of Interplanetary Flights*, Gordon and Breach Publishers, The Netherlands, 1996.

[5] Rauschenbakh, B. V., Ovchinnikov, M. Yu., McKenna-Lawlor, S., *Essential Spaceflight Dynamics and Magnetospherics*, Kluwer Academic Publishers, The Netherlands, 2003.

[6] Chebotarev, G. A. *Gravitational Spheres of the Major Planets, Moon and Sun*, Soviet Astronomy - AJ. Vol. 7, No. 5, 1964, pp. 618-622.

[7] Laplace, P., *Celestial Mechanics*, Chelsea, New York, 1966.

[8] Chobotov V., *Orbital Mechanics*, AIAA Education Series, Virginia, 2002.

[9] Battin, R., *An Introduction to the Mathematics and Methods of Astrodynamics*, AIAA Education Series, Virginia, 1999.

[10] Ross, S. D., Scheeres, D. J., *Multiple Gravity Assists, Capture, and Escape in the Restricted Three-Body Problem*, SIAM J. Applied Dynamical Systems Vol. 6, No. 3, 2007, pp. 576-596.

[11] Hamilton, D. P., Burns, J. A., *Orbital Stability Zones about Asteroids*, Icarus 92, 1991, pp. 118-131.

[12] Roy, A. E., *Orbital Motion*, Adam Hilger Ltd, Bristol, 1982.

[13] Kislik, M. D., *Spheres of Influence of Large Planets and the Moon*, Cosmic Reseach Vol. 2, Issue 6, 1964, pp. 853-858.

[14] Radzievskii, V. V., *Gravitational Capture of Cosmic Dust by the Sun and Planets and Evolution of the Circumterrestrial Cloud*, Soviet Astronomy Vol. 11, No. 1, 1967, pp. 128-136.

[15] Alligood, K. T., Sauer, T. D., Yorke, J.A., *Chaos: An Introduction to Dyanmical Systems*, Springer Verlag, New York, 1996.

[16] Stewart, I., *The Mathematics of Chaos*, Basil Blackwell Ltd, Oxford UK, 1989.

[17] Hilborn, R., *Chaos and Non Linear Dyanmics*, Oxford University Press, New York, NY, 1994.

[18] Lorenz, E. N., *Deterministic Nonperiodic Flow*, Journal of the Atmostpheric Sciences Vol. 20, 1963, pp. 130-141.

[19] Casdagli, M., *Chaos and Deterministic versus Stochastic Non-Linear Modelling*, Journal of the Royal Statistical Society B, Vol. 54, No. 2, 1992, pp. 303-328.

[20] May, R. M., *Simple Mathematical Models with Very Complicated Dynamics*, Nature, Vol. 261, 1976, pp 459-467.

[21] Nonlinear Dynamics and Chaos - A Toolbox for Complex Systems Research, Hubler, A. W., URL: http://www.how-why.com/ph510/LogisticMap_BifurcationDiagram.JPG [cited 24 March 08].

[22] Wikimedia, URL: http://upload.wikimedia.org/wikipedia/commons/f/f4/Lorenz_attractor.svg [cited 25 March 08].

[23] Hedrih, K., *Nonlinear Dynamics and Aleksandr Mikhailovich Lyapunov*, Scientific Technical Review, Vol. 57, No. 1, 2007, pp. 3-7.

[24] Wolf, R. C., *Local Lyapunov Exponents: Looking Closely at Chaos*, Journal of the Royal Statistical Society B, Vol. 54, No. 2, 1992, pp. 353-371.

[25] Tapley, B. D., Schutz, B. E., Born, G. H., *Statistical Orbit Determination*, Elsevier Academic Press, London, 2004.

[26] Bate, R., Mueller D. , White J., *Fundamentals of Astrodynamics*, Dover Publications, New York, 1971.

[27] Chaos on the Web, Cross, M., URL: http://www.cmp.caltech.edu/ mcc/Chaos_Course/Outline.html [cited 30 March 08].

[28] Freedman, R. A., Kaufmann, W. J., *Universe*, W. H. Freeman, New York, 2002.

Appendices

Appendix A

MATLAB Code

A.1 Double Precision Simulation

```
%=============================================================================================%
%                        PROPOGATING THE EC DOUBLE PRECISION STATES                           %
%=============================================================================================%
clear all; close all; clc;
format long; format compact;
path(path,'\Matlab2\m_files')

%================================ SETTING UP THE PROBLEM ================================%

% ———— User Inputs ————
for alt = 359750:50:360250;                 % meters
    for angle = -36.890:-0.008:-36.970;     % degrees
        Δv = 3102.13;                       % m/s
        fprintf('alt = %6.0f , ang = % 6.3f \n', alt, angle);

        t0 = 0;                     % secs
        del_t = 20;                 % secs
        tf = 3.5*86400;             % secs  86400 secs = 1 day

        folder = char(['alt_' int2str(alt) '_ang_' int2str(abs(angle*1000))]);

    % ———— Constants ————
        GMm = 4.90266e12;           % m3/s2
        GMe = 3.98600436e14;        % m3/s2
        radE = 6372797;             % meters
        EMdist = 384400000;         % meters
        omega = sqrt((GMe+GMm)/EMdist^3); % rad/sec
        Tm = 2*pi/omega;            % secs 27d 6h 49m 50.34879957310977s
        alpha = angle*pi/180;       % radians
        h = radE + alt;             % meters
        Vorbit = sqrt(GMe/h);       % m/s
        V = Vorbit + Δv;            % m/s

    % ———— Initial Conditions ————
        rxi =  h*sin(alpha);        % meters
        ryi = -h*cos(alpha);        % meters
        vxi =  V*cos(alpha);        % m/s
        vyi =  V*sin(alpha);        % m/s
        x = [rxi;ryi;vxi;vyi];

%================================ PERFORM THE PROPOGATION ================================%

        % ———— EARTH CENTERED FRAME ————
        frame = 1;
```

```
        xmt = EMdist*cos(omega*t0);
        ymt = EMdist*sin(omega*t0);
        fid = fopen([folder '\DblECI_' int2str(del_t) '.txt'], 'w');
        f = fopen([folder '\DblmoonECI_' int2str(del_t) '.txt'], 'w');
        facc = fopen([folder '\AccECI_' int2str(del_t) '.txt'], 'w');
        fprintf(fid, '% 6.3f, % 6.3f, % 6.3f, % 6.3f, % 6.3f \n', tf/86400, del_t, ...
                alt/1000, Δv, angle);
        fprintf(fid, '% 6.0f, % .16e, % .16e, % .16e, % .16e \n', t0, x);
        fprintf(f, '% 6.0f, % .16f, % .16f \n', t0, xmt, ymt);
        for t = t0+del_t:del_t:tf
           % Use the moon position at the end of the previous interval as the
           % position at the start of this interval.
            xm = xmt;
            ym = ymt;
           % Calculate the moon position at the middle and end of this interval.
            xmh = EMdist*cos(omega*(t + 0.5*del_t));
            ymh = EMdist*sin(omega*(t + 0.5*del_t));
            xmt = EMdist*cos(omega*(t + del_t));
            ymt = EMdist*sin(omega*(t + del_t));
           % Propogating the states forward in time
            [x,accem] = integrate(x, del_t, xm, ym, xmh, ymh, xmt, ymt, frame);
            fprintf(fid, '% 6.0f, % .16e, % .16e, % .16e, % .16e\n',t,x);
            fprintf(f, '% 6.0f, % .16f, % .16f \n', t, xmt, ymt);
            fprintf(facc, '% 6.0f, % .16f, % .16f, % .16f, % .16f, % .16f, % .16f,' ...
                    '% .16f, % .16f \n', t, accem);
        end
        fclose(fid);
        fclose(f);
        fclose(facc);
    end
end
```

A.2 Single Precision Simulation

```
%=============================================================================================%
%                     PROPOGATING THE EC -> MC SINGLE PRECISION STATES                        %
%=============================================================================================%
clear all; close all; clc;
format long; format compact;
path(path,'\Matlab2\m_files')

% ------- User Inputs ------
for alt = 359750:50:360250;             % meters
    fprintf('alt = % 4.4f \n', alt);
    for angle = -36.890:-0.008:-36.970; % degrees
        fprintf('angle = % 4.4f \n', angle);
        Δv = 3102.13;                   % m/s
        t0 = 0;                         % secs
        del_t = 20;                     % secs
        tf = 3.5*86400;                 % secs  86400 secs = 1 day
        for fSPvec = 0.01:0.01:0.99;
            fprintf('fSP = % 4.4f \n', fSPvec);
            fSP = SinglePrec(fSPvec, alt, angle, Δv, t0, del_t, tf);
        end
    end
end
```

```
%================================ SETTING UP THE PROBLEM ================================%
function fSP = SinglePrec(fSP, alt, angle, Δv, t0, del_t, tf)

% ———— User Inputs (from SwPts.m) ————
alt = single(alt);              % meters
angle = single(angle);          % degrees (CCW from the negative y—axis)
Δv = single(Δv);                % m/s
t0 = single(t0);                % secs
del_t = single(del_t);          % secs
tf = single(tf);                % secs  86400 secs = 1 day
fSP = single(fSP);
spt = fSP*100;
tSP = floor(fSP*tf/del_t + 0.5) * del_t;

folder = char(['alt_' int2str(alt) '_ang_' int2str(abs(angle*1000))]);

% ———— Constants ————
GMm = single(4.90266e12);           % m3/s2
GMe = single(3.98600436e14);        % m3/s2
radE = single(6372797);             % meters
EMdist = single(384400000);         % meters
omega = single(sqrt((GMe+GMm)/EMdist^3)); % rad/sec
% Tm = 2*pi/omega = 27d 6h 49m 50.34879957310977s
alpha = single(angle*pi/180);       % radians
h = single(radE + alt);             % meters
Vorbit = single(sqrt(GMe/h));       % m/s
V = single(Vorbit + Δv);            % m/s

% Initial Conditions
rxi =  single(h*sin(alpha));        % meters
ryi = single(—h*cos(alpha));        % meters
vxi =  single(V*cos(alpha));        % m/s
vyi =  single(V*sin(alpha));        % m/s

x = [rxi;ryi;vxi;vyi];

%====================== PERFORM THE PROPOGATION ==========================================%

% ———— EARTH CENTERED FRAME ————
frame = single(1);
xmt = EMdist*cos(omega*t0);
ymt = EMdist*sin(omega*t0);
fid = fopen([folder '\Sgl_' int2str(del_t) '_' int2str(spt) '.txt'], 'w');
f = fopen([folder '\Sglmoon.txt'], 'w');
fprintf(fid, '% 6.3f, % 6.3f, % 6.3f, % 6.3f, % 6.3f, % 6.3f, % 6.3f \n', fSP, tSP,...
        tf/86400, del_t, alt/1000, Δv, angle);
fprintf(fid, '% 6.0f, % .16e, % .16e, % .16e, % .16e \n', t0, x);
fprintf(f, '% 6.0f, % .16f, % .16f \n', t0, xmt, ymt);
for t = t0+del_t:del_t:tSP
   % Use the moon position at the end of the previous interval as the
   % position at the start of this interval.
    xm = xmt;
    ym = ymt;
   % Calculate the moon position at the middle and end of this interval.
    xmh = EMdist*cos(omega*(t + 0.5*del_t));
    ymh = EMdist*sin(omega*(t + 0.5*del_t));
    xmt = EMdist*cos(omega*(t + del_t));
    ymt = EMdist*sin(omega*(t + del_t));
   % Propogating the states forward in time
    x = integrate(x, del_t, xm, ym, xmh, ymh, xmt, ymt, frame);
    fprintf(fid, '% 6.0f, % .16e, % .16e, % .16e, % .16e\n',t,x);
    fprintf(f, '% 6.0f, % .16f, % .16f \n', t, xmt, ymt);
end
```

```
% ————————— SWITCH POINT —————————
% Convert state vector from EC to MC
moon = [xmt;ymt];
xmdot = -EMdist*omega*sin(omega*(t+del_t));
ymdot =  EMdist*omega*cos(omega*(t+del_t));
mndot = [xmdot;ymdot];
x = x-[moon;mndot];

% ———————— MOON CENTERED FRAME ————————
frame = single(2);
for t = tSP+del_t:del_t:tf
   % Use the moon position at the end of the previous interval as the
   % position at the start of this interval.
    xm = xmt;
    ym = ymt;
   % Calculate the moon position at the middle and end of this interval.
    xmh = EMdist*cos(omega*(t + 0.5*del_t));
    ymh = EMdist*sin(omega*(t + 0.5*del_t));
    xmt = EMdist*cos(omega*(t + del_t));
    ymt = EMdist*sin(omega*(t + del_t));
   % Compute moon state at end of interval
    moon = [xmt;ymt];
    mndot = EMdist*omega*[-sin(omega*(t + del_t));cos(omega*(t + del_t))];
   % Propogating the states forward in time
    x = integrate(x, del_t, xm, ym, xmh, ymh, xmt, ymt, frame);
   % Compute the EC state from the MC state
    xeci = x+[moon;mndot];
    fprintf(fid, '% 6.0f, % .16e, % .16e, % .16e, % .16e\n',t,xeci);
    fprintf(f, '% 6.0f, % .16f, % .16f \n', t, xmt, ymt);
end
fclose(fid);
fclose(f);
```

A.3 Sub-Routines

```
%=========================================================================================%
%                   M-FILES USED FOR TRAJECTORY PROPOGATION SUB-ROUTINES                  %
%=========================================================================================%
function [xnew,accem] = integrate(x, del_t, xm, ym, xmh, ymh, xmt, ymt, frame)

% ——— Perform a 4th Order Runge-Kutta Integration ———
x0 = x;
x0dot = deriv(x0,xm,ym,frame);
x1 = x0 + 0.5*del_t*x0dot;
x1dot = deriv(x1,xmh,ymh,frame);
x2 = x0 + 0.5*del_t*x1dot;
x2dot = deriv(x2,xmh,ymh,frame);
x3 = x0 + del_t*x2dot;              % No 0.5 factor
x3dot = deriv(x3,xmt,ymt,frame);
x4 = x0 + del_t/6.0*((x0dot+x3dot) + 2.0*(x1dot+x2dot));
xnew = x4;

% ——— Calculate the seperate acceleration components ———
% ———————— of the vehicle due to the earth and moon ————————
accem = acc(x,xm,ym);
```

```
%=========================================================================================%
function xdot = deriv(x,xm,ym,frame)

GMm = 4.90266e12;       % m3/s2
GMe = 3.98600436e14;    % m3/s2
pos = x(1:2);  rv = pos;
vel = x(3:4);
moon = [xm;ym];  rm = moon;

if frame == 1           % For Earth Centered Frame
    acc = -GMe*rv/nrm(rv)^3 - GMm*((rv-rm)/nrm(rv-rm)^3 + rm/nrm(rm)^3);
elseif frame == 2       % For Moon Centered Frame
    acc = -GMm*rv/nrm(rv)^3 - GMe*((rv+rm)/nrm(rv+rm)^3 - rm/nrm(rm)^3);
end
xdot = [vel;acc];

%=========================================================================================%
function accem = acc(x,xm,ym)

GMm = 4.90266e12;       % m3/s2
GMe = 3.98600436e14;    % m3/s2
pos = x(1:2);  rv = pos;
moon = [xm;ym];  rm = moon;
d=rv-moon;

acce_EC = GMe*rv/nrm(rv)^3;
accm_EC = GMm*((rv-rm)/nrm(rv-rm)^3 + rm/nrm(rm)^3);
% ratioEC = norm(accm_EC)/norm(acce_EC);

accm_MC = GMm*d/nrm(d)^3;
acce_MC = GMe*((pos)/nrm(pos)^3 - rm/nrm(rm)^3);
% ratioMC = norm(acce_MC)/norm(accm_MC);

accem = [acce_EC' accm_EC' accm_MC' acce_MC'];
% ratio = [ratioEC ratioMC];

%=========================================================================================%
function N = nrm(vec)
N = sqrt(sum(vec.^2));
```

Appendix B
Historical Review

B.1 Claudius Ptolemaeus

Ptolemaeus (circa 100 - 170 AD), better known as Ptolemy, was a Greek astronomer, mathematician and geographer. He expanded upon the work of Hipparchus and codified the geocentric model of the universe using *epicycles* and *deferents*. The astronomical data in the library at Alexandria enabled Ptolemy to deduce the sizes and rotation rates of the epicycles and deferents of the Sun, Moon and planets. Much of his work is assembled in the 13 volume treatise known as the *Almagest*.

B.2 Nicolaus Copernicus

Copernicus (1473 - 1543), a Polish lawyer, physician, mathematician and astronomer, was a strong proponent of the heliocentric model of the universe, although he still considered all planets on circular orbits. His seminal work, *De Revolutionibus Orbium Coelestium*, was not published until after his death, and remained on the index of forbidden books from 1616 - 1758.

B.3 Galileo Galilei

Galileo (1564 - 1642), born in Pisa, Italy, was one of the first people to use a telescope to observe the heavens. He discovered craters on the Moon, sunspots on the Sun, the rings of Saturn, the phases of Venus and four moons orbiting Jupiter. His discoveries strongly suggested a heliocentric structure of the universe, which contradicted the prevailing opinion of the time. As such, he spent the last eight years of his life under house arrest for suspicion of heresy.

B.4 Johannes Kepler

Kepler (1571 - 1630) was a German mathematician and astronomer. He was a supporter of the Copernican heliocentric model, but introduced the idea of elliptic orbits of the planets. Using the observations of Tycho Brahe, which are credited as

being the most accurate of the time, Kepler was able to develop the modern laws of planetary motion.

B.5 Isaac Newton

Newton (1642 - 1727) was born in Lincolnshire county, England and is considered by some people to have been the most influential person in the history of science. Among many other things, he is credited with inventing the reflecting telescope, formulating an empirical law of cooling and shares credit with Gottfried Leibniz for the development of calculus. Perhaps his must significant contribution to science however include his three laws of motion and his law of universal gravitation. Although twentieth century scientists found that Newton's laws break down in certain situations (on atomic and relativistic scales), Newtonian mechanics has become the cornerstone of modern physical science.

B.6 Joseph Louis Lagrange

Lagrange (1736 - 1813), born in Torino, Italy, introduced key concepts and developed innovative methods in mathematical analysis, differential equations, number theory and classical and celestial mechanics. His 1788 treatise on analytical mechanics, *Mécanique Analytique*, offered the most comprehensive treatment of classical mechanics since Isaac Newton. His attempts to solve the three-body problem resulted in the discovery of the Lagrangian points in 1772. He also predicted the existence of (Trojan) asteroids at the triangular libration points of the Sun-Jupiter system 134 years before astronomical observations confirmed their existence.

B.7 Pierre-Simon Laplace

Laplace (1749 - 1827) was born in Normandy, France, and became a professor at the École Militaire in Paris at the age of 18. Some of his major contributions include the formulation of Laplace's equation, inventing the Laplace transform, introducing the concept of the potential function and his work on the stability of the solar system. He was also one of the first scientists to postulate the existence of black holes, and his seminal work *Mécanique Céleste* helped transform the study of classical mechanics from a geometry based study to one based on calculus.

B.8 Henri Poincaré

Poincaré (1854 - 1912) was a French mathematician and physicist who established the concept of non-integrable dynamical systems. One of Poincaré's major works on celestial mechanics includes *Les Méthodes Nouvelles de la Mécanique Céleste*, in which he aimed to completely characterize all motions of mechanical systems. His work helped lay the foundation of modern chaos theory, as well as the the field of topology. He is acknowledged as a co-discoverer, with Albert Einstein and Hendrik Lorentz, of the special theory of relativity. There is now a mathematical institute in Paris that is named after him.

B.9 Aleksandr Lyapunov

Lyapunov (1857 - 1918) received his early education from his father, Mikhail Lyapunov, a well known Russian Astronomer. In 1876, he entered Saint Petersburg State University where he published two papers on hydrostatics during his fourth year. After successfully defending his doctoral thesis on *The general problem of the stability of motion* in 1892, he was appointed as a professor at Kharkov University. He remained there for almost a decade, and in 1901 was elected as a member of the Russian Academy of Sciences. Much of his work focussed on the stability of systems, and probability theory. Today his name is found in many areas of mathematics such as Lyapunov fractal, Lyapunov function, Lyapunov equation, Lyapunov stability and the Lyapunov exponent.

Apollo, 1
Astrodynamics, 4

Bifurcation, 23
Butterfly Effect, 21

Celestial Mechanics, 4, 7, 10
Chaos, 7, 21, 36, 43, 47

Deterministic, 22
Dynamics, 4, 22, 29

Eigenvalue, 30, 37
Ergodic Theory, 21
Error
    Discretization, 1, 34, 47
    Iterative, 1, 34
    Round-off, 1, 34, 35, 38, 46

Gravitational Constant, 4

Hill Sphere, 15

Jacobi's Integral, 15, 17

Kepler, Johannes, 32, 56
King Oscar II, 6

Lagrange Points, 17
Laplace, Pierre-Simon, 12, 57
Lorenz Attractor, 24
Lorenz, Edward, 20
Low Earth Orbit, 1, 34
Lyapunov
    Aleksandr, 25
    Exponent, 25, 28, 30, 36, 43
Lyapunov Exponent, 47
Lyapunov, Aleksandr, 58

Map, 22, 25, 28
Mean Motion, 18

Newton
    Law of Gravitation, 4, 5
    Law of Motion, 3, 6
Newton, Isaac, 3, 57

Patched-Conic Approximation, 10
Perturbation, 9, 21, 32, 35, 38
Poincaré, Henri, 7, 21, 58
Project Constellation, 1

Runge-Kutta, 33, 46

Sensitivity, 21, 47
Sphere
    Hill, 44
    Kislik, 17, 44
    of Influence, 12, 44
State Transition Matrix, 29, 37
Stochastic, 22

Three-Body Problem, 7, 31
Two-Body Problem, 4, 6, 10

Verholst, Pierre François, 23

Weierstrass, Karl, 7

Zero Velocity Curves, 16